



LUND UNIVERSITY

**Semi-Analytical Finite  
Element method for guided  
waves in civil engineering  
plate-like structures**

Christian Nielsen

2015

Master's Thesis

ISRN LUTVDG / (VTG-5140) / 1-86 (2015)

Division of Engineering Geology  
Faculty of Engineering  
Lund University

Supervisors: Nils Rydén and Oskar Baggens



# Abstract

Guided waves have a significant potential for Structural Health Monitoring (SHM) and Non-Destructive Testing (NDT) due to their relatively long distance of propagation and sensitivity to discontinuities along the propagation path, anywhere through the material thickness. The inability to model wave guides of arbitrary cross-section using current matrix methods, has led to the development of a technique called Semi-Analytical Finite Element (SAFE).

In civil engineering it is of considerable interest to study guided waves in plates and plate-like structures: such as foundations, embankments, reactor enclosures and dams. NDT have potential as an essential tool in the life cycle management of the built environment: from preliminary investigations, verification of new structures to its maintenance and, finally, demolition.

In this master's thesis the semi-analytical finite element method is reviewed, implemented and studied for civil engineering plate-like structures using the commercial finite element software COMSOL. First, a review of SAFE and its underlying concepts, such as solid mechanics, Lamb waves and quadratic eigenvalue problems, is presented. Second, its implementation, using a coefficient form *Partial Differential Equation* (PDE) formalism in COMSOL's mathematical modelling environment, is presented. Third, SAFE is applied to four civil engineering problems: (1) a continuous homogeneous isotropic linear elastic free plate, (2) a continuous homogeneous isotropic linear elastic free plate with proportional hysteretic damping, (3) a continuous isotropic linear elastic free plate with a stiffness gradient and (4) a multi-layered half-space.

The SAFE model solution is curve fitted to synthetic data from the matrix method software DISPERSE.

It is found that SAFE successfully predicts the dispersion relations for the enumerated civil engineering structures. Furthermore, it is shown that exploiting the underlying eigenvalues and eigenvectors, extended properties such as attenuation, lossless excitability and energy velocity may be predicted using a SAFE formulation. Moreover, it is shown that introducing light damping to a free plate results in negligible changes in phase velocities. Furthermore, it is shown that a stiffness gradient over the plate thickness have small effects on the  $S_1$  zero group velocity frequency.

# Contents

|   |           |
|---|-----------|
| <b>Abstract</b>                                       | <b>3</b>  |
| <b>1 Introduction</b>                                 | <b>7</b>  |
| 1.1 Field of research . . . . .                       | 7         |
| 1.2 Motivations of work . . . . .                     | 9         |
| 1.3 Aim and objective . . . . .                       | 9         |
| <b>2 Solid mechanics</b>                              | <b>11</b> |
| 2.1 Strain measurement . . . . .                      | 11        |
| 2.2 Stress measurement . . . . .                      | 11        |
| 2.3 Stress-Strain relation . . . . .                  | 12        |
| 2.3.1 Isotropic medium . . . . .                      | 12        |
| 2.4 Damping models . . . . .                          | 13        |
| <b>3 Guided waves</b>                                 | <b>17</b> |
| 3.1 Equations of motion . . . . .                     | 17        |
| 3.2 Guided waves in isotropic medium . . . . .        | 20        |
| 3.2.1 Propagation in a free isotropic plate . . . . . | 21        |
| <b>4 SAFE method</b>                                  | <b>27</b> |
| 4.1 Mathematical preliminaries . . . . .              | 28        |
| 4.1.1 Quadratic Eigenvalue Problems . . . . .         | 28        |
| 4.1.2 SAFE mathematical framework . . . . .           | 30        |
| 4.1.3 FE-discretisation . . . . .                     | 32        |
| 4.1.4 Solutions to undamped medium . . . . .          | 35        |
| 4.1.5 Solutions to damped medium . . . . .            | 36        |
| 4.2 Comsol Multiphysics . . . . .                     | 36        |

|  |           |
|--|-----------|
| <b>5 Case Studies</b>  | <b>39</b> |
| 5.1 Modelling process . . . . .  | 39        |
| 5.2 Solving for a continuous homogeneous isotropic linear elastic free plate . . . . . | 41        |
| 5.2.1 2D SAFE Implementation . . . . .   | 41        |
| 5.2.2 1D SAFE Implementation . . . . .   | 43        |
| 5.2.3 Results . . . . .  | 43        |
| 5.3 Extended properties for guided wave propagation . . . . .                          | 46        |
| 5.3.1 Group and energy velocity . . . . .  | 46        |
| 5.3.2 Lossless Excitability . . . . .  | 47        |
| 5.3.3 1D SAFE Implementation . . . . .   | 47        |
| 5.3.4 Results . . . . .  | 48        |
| 5.4 Effects of damping . . . . .   | 51        |
| 5.4.1 1D SAFE Implementation . . . . .   | 51        |
| 5.4.2 Results . . . . .  | 52        |
| 5.5 Effects of stiffness gradient . . . . .  | 56        |
| 5.5.1 1D SAFE Implementation . . . . .   | 56        |
| 5.5.2 Results . . . . .  | 57        |
| 5.6 Leaky characteristics and unbounded domains . . . . .                              | 61        |
| 5.6.1 1D SAFE Implementation . . . . .   | 63        |
| 5.6.2 Results . . . . .  | 64        |
| <b>6 Summary</b>   | <b>69</b> |
| 6.1 Discussion . . . . .   | 69        |
| 6.2 Conclusions . . . . .  | 72        |
| 6.3 Future work . . . . .  | 74        |
| <b>Appendix: Source Code</b>   | <b>81</b> |
| Sample Source Code: 1D SAFE . . . . .  | 81        |

# Chapter 1

## Introduction

### 1.1 Field of research

Non-Destructive Testing (NDT) is a “general term which refers to the task of evaluating some sort of property without introducing any permanent damage on the studied object” ([Baggens, 2015](#)). Within the field of non-destructive testing there exists a wide variety of methods, spanning different fields of physics: from electromagnetism, through resistivity to acoustics. In this thesis we’ll consider guided acoustic waves in a solid. In other words, mechanical waves travelling along some boundary or interface in a solid. From the perspective of civil engineering, it is of considerable interest to study wave propagation in plate-like structures.

Wave propagation in plates were first studied by Horace [Lamb \(1917\)](#), who developed an analytical solution to the simplest plate structure in which guided waves can propagate: a free homogeneous isotropic linear elastic plate. Other plates, as well as other wave guides, share some important phenomena with the idealized free plate, namely that the propagation, fundamentally, is modal and dispersive. Guided waves have been used to determine plate properties such as thickness, Poisson’s ratio and Young’s modulus ([Baggens, 2015](#)), assessing the stiffness of adhesive bonds ([Fan et al., 2013](#)) and estimating the quality of a weld in a steel plate ([Fan and Lowe, 2009](#)).

Conventional ultrasonic inspection systems uses high frequency (i.e. short wavelength) bulk waves to perform line scans (A-scan), that may be combined to create an image of the inspected body ([Baggens, 2015](#)). For concrete structures such measurements are typically performed in the frequency range of 20 kHz to 500 kHz ([Malhotra and Carino, 2004](#)). A guided wave inspec-

tion system, typically, operate at lower frequencies (i.e. longer wavelength). Hence, the wavelength is such that the wave interacts with the boundaries of the wave guide to create a characteristic wave pattern directed along the wave guide - a *guided wave*.

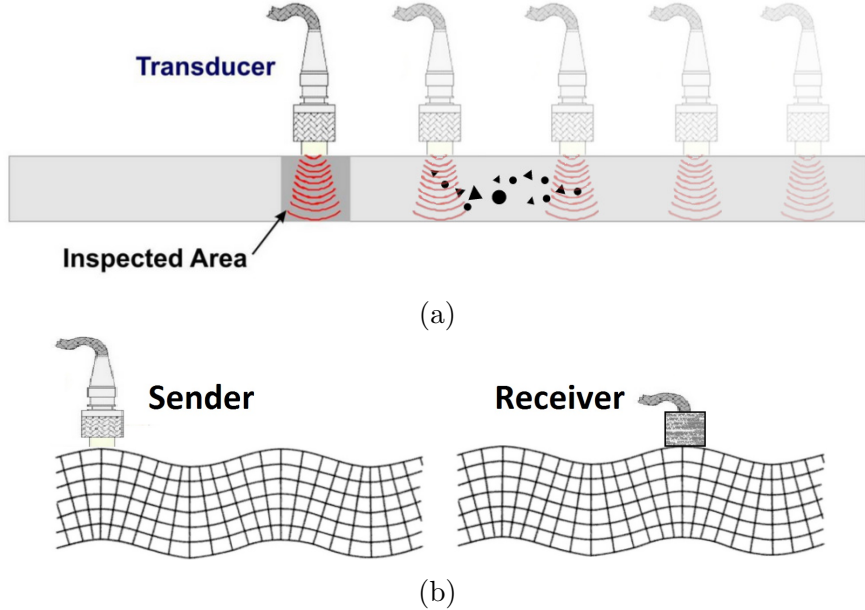


Figure 1.1: (a) Transducer used in high frequency range, and (b) transducer used in guided waves inspection. Picture (a) taken from Sprialboy, CC BY-SA 3.0. Picture (b) taken from [Kuttruff \(1998\)](#).

The benefits of using an inspection system based on guided waves over a conventional ultrasonic inspection system, lies in utilizing the guided waves to reduce a 2D scan of the structure into a 1D scan. In other words, where a conventional system (A-scan) requires the operator to move the probe over the inspection area to perform a series of line scans in the thickness direction, the use of guided waves allows one to inspect the entire thickness for a given length of the wave guide from a single location, see Figure 1.1 ([Wilcox et al., 2001](#)). Additionally, guided waves may propagate over long distances. Consequently, the use of guided waves allows for a long inspection range, which is ideally suited for NDT of elongated structures, such as pipelines ([Lowe et al., 1998](#)). However, an increased inspection range implies a gradually decreasing resolution with distance. Hence, guided waves is preferably used to perform a *global* inspection of the wave guide to approximately locate some feature (e.g. damage). Whereas, conventional ultrasound is preferably

used to perform a *local* inspection, to gain a detailed picture of that feature ([Baggens, 2015](#)).

## 1.2 Motivations of work

When doing inspection measurements, it is of interest to develop a *conceptual model* of the structure in question. For plates, and other wave guides, this, typically, includes estimating the theoretical wave motion modality and dispersivity. Thereby, the inspection system may be optimised for a limited frequency range, and the dominant modes within that range. For the idealized free plate there exist an analytical solution. However, for increasingly complex geometries and material models, these relations do not hold. Using the principle of superpositioning of shear- and pressure waves, various matrix techniques ([Lowe, 1995](#)) were developed to model guided waves in layered media. These techniques have been applied to problems of a broad range of length scales: from thin film coatings to global seismology ([Rydén, 2004](#)). These techniques have been utilized in creating the software **DISPERSE** ([Pavlakovic et al., 1997](#)), a commonly used research tool for modelling plates. However, the root searching algorithm associated with these techniques may miss solutions ([Lowe, 1995](#)). Further developments within modelling yielded the Semi-Analytical Finite Element (SAFE), also referred to as the spectral- or wave guide finite element, as an alternative to the matrix techniques. SAFE methods allowed the study of wave guides of arbitrary cross-sectional geometry. Furthermore, its governing equations yielded a stable eigenvalue problem, and, thus, didn't suffer the problem of missing roots. SAFE has since been successfully used to model a wide variety of structures, such as: rails ([Hayashi et al., 2003](#)), periodic structures ([Predoi et al., 2007](#)) and composite plates ([Ahmad et al., 2013](#)). The new capabilities afforded by the development of SAFE, and its potential application to civil engineering problems, serve as motivation to this master thesis.

## 1.3 Aim and objective

The aim of this master thesis is to implement and study the capabilities of the Semi-Analytical Finite Element (SAFE) method for civil engineering plate-like structures. The work is focused on computing dispersion relations and extended properties such as: attenuation, lossless excitability and energy velocity, using the commercial finite element software **COMSOL**. The results from the implemented SAFE models will be validated against matrix method

solutions for laterally infinite layered plates, from the software **DISPERSE**.

# Chapter 2

## Solid mechanics

### 2.1 Strain measurement

The relevant strain measure when considering an isotropic linear elastic solid, where the displacement length scale and domain length scale differ by an order of magnitude, is the elastic strain tensor for small strains. It will hence be referred to as the strain tensor. Let  $u(x_i, t)$  be the three dimensional displacement vector for a given point  $P$  described by the position vector  $x_i = (x_1, x_2, x_3)$  at time  $t$ . The strains in the vicinity of  $P$  is given by the strain tensor,

$$\varepsilon_{ij} = \frac{1}{2} \left( \frac{\partial u_i}{\partial x_j} + \frac{\partial u_j}{\partial x_i} \right). \quad (2.1)$$

The strain tensor is symmetric and contains six independent components:  $\varepsilon_{11}$ ,  $\varepsilon_{22}$ ,  $\varepsilon_{33}$ ,  $\varepsilon_{12}$ ,  $\varepsilon_{13}$  and  $\varepsilon_{23}$ . In the contracted notation (Voigt-notation) the strain vector is given as:

$$\boldsymbol{\varepsilon} = \begin{bmatrix} \varepsilon_{11} \\ \varepsilon_{22} \\ \varepsilon_{33} \\ 2\varepsilon_{23} \\ 2\varepsilon_{13} \\ 2\varepsilon_{12} \end{bmatrix} = \begin{bmatrix} \varepsilon_1 \\ \varepsilon_2 \\ \varepsilon_3 \\ \gamma_{23} \\ \gamma_{13} \\ \gamma_{12} \end{bmatrix}. \quad (2.2)$$

### 2.2 Stress measurement

The corresponding stress quantity for the small strains tensor is the Cauchy stress tensor. It will hence be referred to as the stress tensor  $\sigma_{ij}$ . Similarly

to the strain tensor it contains six independent components, and is given in the contracted notation as,

$$\boldsymbol{\sigma} = [\sigma_{11} \ \sigma_{22} \ \sigma_{33} \ \sigma_{23} \ \sigma_{13} \ \sigma_{12}]^T. \quad (2.3)$$

## 2.3 Stress-Strain relation

In general, the relation between stress and strain tensor is given by the fourth order elasticity tensor  $C_{ijkl}$ . This relationship is called the materials constitutive relation, such that,

$$\sigma_{ij} = C_{ijkl}\varepsilon_{kl}, \quad (2.4)$$

where the following symmetric properties hold:

$$C_{ijkl} = C_{jikl} = C_{klij} = C_{ijlk}.$$

Thus, the general elasticity matrix contains 21 independent components.

### 2.3.1 Isotropic medium

For a homogeneous, isotropic linear elastic material the number of independent elastic constants reduces to two. Let  $\lambda$  and  $\mu$  be the Lamé parameters for the given material. Then  $C_{ijkl}$  may be expressed as,

$$C_{ijkl} = \lambda\delta_{ij}\delta_{kl} + \mu(\delta_{ik}\delta_{jl} + \delta_{il}\delta_{jk}), \quad (2.5)$$

where  $\delta$  is Kronecker's delta. Therefore, the constitutive relation reduces to Hooke's law, that expressed in the Lamé parameters is given by,

$$\sigma_{ij} = \lambda\varepsilon_{kk}\delta_{ij} + 2\mu\varepsilon_{ij}. \quad (2.6)$$

Other elastic constants; such as Young's modulus  $E$ , shear modulus  $G$ , bulk modulus  $B$  and Poisson's ratio  $\nu$  may be expressed in the Lamé constants by,

$$E = \frac{\mu(3\lambda + 2\mu)}{\lambda + \mu}; \quad \nu = \frac{\lambda}{2(\lambda + \mu)}; \quad B = \lambda + \frac{2\mu}{3}; \quad G = \mu.$$

Inversely, the Lamé constants may be expressed in Young's modulus and Poisson's ratio,

$$\lambda = \frac{\nu E}{(1 + \nu)(1 - 2\nu)}; \quad \mu = \frac{E}{2(1 + \nu)},$$

(Achenbach, 1973). In the contracted notation the elasticity matrix, given in the material parameters  $E$  and  $\nu$ , is

$$[\mathbf{C}_{mn}] = \frac{E}{(1+\nu)(1-2\nu)} \begin{bmatrix} 1-\nu & \nu & \nu & 0 \\ \nu & 1-\nu & \nu & \\ \nu & \nu & 1-\nu & \\ & & & \frac{1}{2}(1-2\nu) \\ 0 & & & \frac{1}{2}(1-2\nu) \\ & & & \frac{1}{2}(1-2\nu) \end{bmatrix}$$

## 2.4 Damping models

Elasticity theory presumes that, during deformation, a material stores energy with no dissipation. However, there always exists some process whereby wave energy is lost and the displacement amplitude is reduced. One such processes is damping. It should be noted that damping as a physical phenomenon isn't totally understood. Thus, all damping models are mathematical representations of observed attenuations, not a fundamental description of underlying physical processes (Sondipon, 2000).

Let's consider two damping models: viscous damping and hysteretic damping. Viscous damping combines the velocity dependent energy dissipation of viscous fluids (dashpot) with the displacement dependent energy-storing capacity of elastic solids (spring), see Figure 2.1. Springs and dashpots may be combined in various forms to model the attenuation. Commonly used models are the Maxwell, Kelvin-Voigt and Standard Linear Solid models . Modern composite and polymer materials are groups of material with considerable viscoelastic damping (Rose, 1999).

Hysteretic damping is based on the concept of internal friction within a material. The energy loss is constant for a load cycle, and is represented by the hysteresis loop in Figure 2.2.b.

Let's consider a harmonic wave motion,

$$\varepsilon = \hat{\varepsilon} e^{i(kx - \omega t)},$$

where the stresses are given by a complex valued elasticity tensor,

$$C_{ijkl} = C'_{ijkl} + iC''_{ijkl}, \quad (2.7)$$

where the real part represent the elastic energy storing capacity, while the imaginary part represent the attenuating capacity. For viscous damping, the

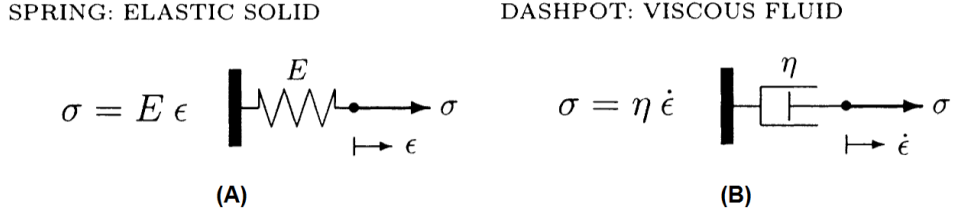


Figure 2.1: SDOF representation of (a) spring and (b) dashpot stresses. Picture taken from [Özkaya et al. \(2012\)](#).

viscous stresses for a SDOF are given by

$$\sigma^V = \eta \dot{\varepsilon},$$

where  $\eta$  is the coefficient of viscosity, see Figure 2.1. This may be generalised to a three dimensional case as,

$$\sigma_{ij}^V = \eta_{ijkl} \dot{\varepsilon}_{kl},$$

where  $\eta_{ijkl}$  is the viscosity tensor. Let's consider a simple viscous model like the Kelvin-Voigt model, see Figure 2.2a. The attenuation becomes linearly dependent on the angular frequency  $\omega$ ,

$$C''_{ijkl} = \omega \eta_{ijkl}.$$

For the hysteretic damping the energy loss should be independent of frequency. Hence,  $C''_{ijkl}$  becomes a constant real valued tensor

$$C''_{ijkl} = \zeta_{ijkl}.$$

Consequently, the attenuation, here the energy loss per unit length, becomes a linear function in  $\omega$  for hysteretic damping and quadratic for viscous damping, see Figure 2.2c. For practical applications  $C''_{ijkl}$  is experimentally defined at a characteristic frequency. Therefore, as long as the working frequencies doesn't differ greatly from the characteristic frequency, the difference between the models is small ([Neau, 2003](#)).

A proportionally damped system is a system where the damping is given as a linear combination of the mass and stiffness distribution,

$$C \propto c_1 M + c_2 K,$$

where  $C$  is the damping matrix,  $M$  is the mass matrix,  $K$  is the stiffness matrix and  $c_1, c_2$  are constants. For proportional damping the mode shapes

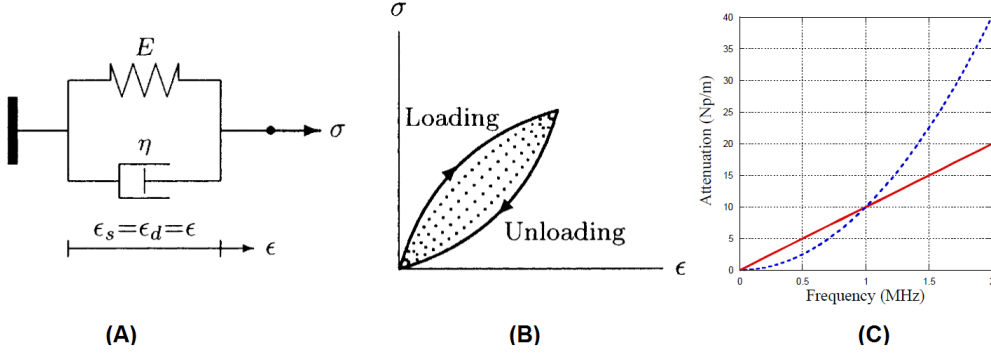


Figure 2.2: (a) Kelvin-Voigt model. (b) Hysteresis loop. (c) Comparison between hysteretic damping (solid line) and viscous Kelvin-Voigt damping (dotted line) characterised for an arbitrary material at 1 MHz. Picture (a) and (b) taken from [Özkaya et al. \(2012\)](#). Picture (c) taken from [Neau \(2003\)](#).

of both viscous and hysteretic damping are the same as those of the corresponding undamped system. Due to different normalization schemes of the mode shapes (eigenvectors) corresponding to the different damping models, the mode shapes may appear different, in both phase and amplitude. However, the mode shapes of the different models are mapped onto one another by a scaling factor. An approximative scaling factor may be derived for non-proportional damping as well, with a small error in the corresponding mapping ([Lin and Zhu, 2009](#)). In brief it may be said that errors due to choice of a particular damping model over another, are small. Furthermore, it should be noted that in real structures material damping, typically, is negligible compared to damping occurring at joints. In this thesis we'll consider all material interfaces as perfectly coupled and thus only material damping will come into play.



# Chapter 3

## Guided waves

Guided waves occur along an interface, typically, and is unbounded in one or two dimensions. In this chapter we'll start by considering the equations of motion and bulk waves in an isotropic solid. Guided waves is a special case of the equations of motion where the application of different boundary conditions yields a variety of different wave types. We'll limit ourselves to considering the isotropic free plate, which give rise to Lamb waves.

### 3.1 Equations of motion

The wave equation for an isotropic elastic solid is derived from Newton's second law. Let's consider an infinitesimal cubic element  $\Omega$  with the density  $\rho$ . Hence, Newton's law may be formulated as,

$$\rho \ddot{u}_i = \sigma_{ij,j} + b_i \quad (3.1)$$

where  $b_i$  are the distributed body forces. If the body forces are neglected, i.e.  $b_i = 0$ , equation (3.1) may be written explicitly as,

$$\rho \frac{\partial^2 u_1}{\partial t^2} = \frac{\partial \sigma_{11}}{\partial x_1} + \frac{\partial \sigma_{12}}{\partial x_2} + \frac{\partial \sigma_{13}}{\partial x_3},$$

$$\rho \frac{\partial^2 u_2}{\partial t^2} = \frac{\partial \sigma_{21}}{\partial x_1} + \frac{\partial \sigma_{22}}{\partial x_2} + \frac{\partial \sigma_{23}}{\partial x_3},$$

$$\rho \frac{\partial^2 u_3}{\partial t^2} = \frac{\partial \sigma_{31}}{\partial x_1} + \frac{\partial \sigma_{32}}{\partial x_2} + \frac{\partial \sigma_{33}}{\partial x_3}.$$

Substitution of equations (2.1) and (2.4) into (3.1), yields

$$\rho \ddot{u}_i = C_{ijkl} \frac{1}{2} (u_{l,kj} + u_{k,lj}). \quad (3.2)$$

Due to the symmetry of the strain tensor, we may consider  $l$  and  $k$  as interchangeable, hence, we can simplify (3.2) as,

$$\rho \ddot{u}_i = C_{ijkl} u_{k,lj} \quad (3.3)$$

Equation (3.3) is the *displacement equations of motion* (Achenbach, 1973). It is the most general form of wave equation. It must be satisfied for all elastic oscillations at every interior point of a body (Rydén, 2004; Achenbach, 1973). Solutions to the displacement field  $u_i$  are typically proposed as,

$$u_i = U_i e^{i(k\vec{n}_j x_j - \omega t)}$$

where  $U_i$  is the displacement amplitude field,  $k$  is the wave number,  $\vec{n}$  is the propagation direction unit vector,  $i = \sqrt{-1}$  and  $\omega$  is the angular frequency.

Let's consider the displacement equations of motions for an isotropic medium, by substitution of equation (2.5) into (3.3),

$$\rho \ddot{u}_i = \mu u_{i,jj} + (\lambda + \mu) u_{j,ji} \quad (3.4)$$

or in vector form:

$$\rho \ddot{\mathbf{u}} = \mu \nabla^2 \mathbf{u} + (\lambda + \mu) \nabla (\nabla \cdot \mathbf{u}) \quad (3.5)$$

There is a drawback to the displacement equations of motions. It is an equation system where the three displacement components are coupled, hence it is difficult to solve. One may uncouple the system by eliminating two displacement components by insertion. However, this yields a sixth order differential equation (Achenbach, 1973). Instead, the components may be expressed in terms of two potentials: a scalar potential  $\phi$  and a vector potential  $\psi$ ,

$$\mathbf{u} = \nabla \phi + \nabla \times \psi. \quad (3.6)$$

This is the Helmholtz decomposition of the displacement vector field  $\mathbf{u}$  into a rotational, divergence free, vector field  $\nabla \times \psi$  and irrotational vector field  $\nabla \phi$ . Where  $\psi$  has zero divergence,

$$\nabla \cdot \psi = 0. \quad (3.7)$$

Substitution of the decomposition (3.6) into Equation (3.5) yields:

$$\rho \frac{\partial^2}{\partial t^2} (\nabla \phi + \nabla \times \boldsymbol{\psi}) = \mu \nabla^2 (\nabla \phi + \nabla \times \boldsymbol{\psi}) + (\lambda + \mu) \nabla (\nabla \cdot [\nabla \phi + \nabla \times \boldsymbol{\psi}]) . \quad (3.8)$$

Since  $\nabla \cdot \nabla \phi = \nabla^2 \phi$  and  $\nabla \cdot \nabla \times \boldsymbol{\psi} = 0$ , one obtains through rearrangement,

$$\nabla \left[ (\lambda + \mu) \nabla^2 \phi - \rho \ddot{\phi} \right] + \nabla \times \left[ \mu \nabla^2 \boldsymbol{\psi} - \rho \ddot{\boldsymbol{\psi}} \right] = 0 . \quad (3.9)$$

Obviously, this equation is satisfied if the quantities within the square brackets are zero. Hence the solution to (3.9) satisfies,

$$\nabla^2 \phi = \frac{1}{c_L^2} \ddot{\phi} , \quad (3.10)$$

and

$$\nabla^2 \boldsymbol{\psi} = \frac{1}{c_T^2} \ddot{\boldsymbol{\psi}} , \quad (3.11)$$

where

$$c_L^2 = \frac{\lambda + 2\mu}{\rho} ; \quad c_T^2 = \frac{\mu}{\rho} .$$

The first solution (3.10) represents an irrotational part of the displacement field (Achenbach, 1973). This is the longitudinal wave, and is also called compression wave. Longitudinal waves propagate by particle displacement parallel to the direction of propagation,  $\mathbf{u} \parallel \vec{\mathbf{n}}$ . Longitudinal waves are the fastest mechanical waves, thus its also called *primary wave* or P-wave (Rydén, 2004). The second solution (3.11) represents the divergence free part of the displacement field (Achenbach, 1973). This is the transversal wave, and is also called shear wave. Transversal waves propagate by particle motions perpendicular to the direction of propagation,  $\mathbf{u} \perp \vec{\mathbf{n}}$ . The transversal wave is slower than the P-wave and is, thus, also called *secondary wave* or S-wave. This shows that there are only two types of wave propagation in the interior of the body: P-waves and S-waves. These are called *bulk waves* or *body waves*, in contrast to wave propagating along a free boundary, *surface waves*, or some material interface, *interface waves*. Guided waves is a general term including both surface waves and interface waves. Note that pure P- and S-waves only occur in an unbounded medium or media much larger than a wave length (Rydén, 2004). When the modes are not pure they are typically described as quasi-longitudinal or quasi-shear waves (Auld, 1973).

## 3.2 Guided waves in isotropic medium

Previously, we considered the wave equations in an unbounded medium. However, the presence of discontinuities, typically material boundaries, have significant influence on the wave propagation. At the boundary interface *refraction* and *reflection* of the incident wave occurs. For the case of a boundary between a medium that transmits mechanical waves and one that doesn't, i.e. between some material and vacuum, there occurs only reflection (Achenbach, 1973). Wave propagation in a bounded media may be modelled based on superposition of incident, refracted and reflected P- and S-wave if appropriate boundary conditions are considered (Rydén, 2004). Hence, we may describe the propagation in semi-infinite half-spaces, layered media and plates.

Let's consider a plane wave, where the wave motion is independent of the coordinate  $x_2$ . This corresponds to motion in plain strain in the  $x_1$ - $x_3$ -plane, i.e. out-of-plane displacements are zero,  $u_2 = 0$ . Consequently, the wave equations (3.10) and (3.11) may be written as:

$$\frac{\partial^2 \phi}{\partial x_1^2} + \frac{\partial^2 \phi}{\partial x_3^2} = \frac{1}{c_L^2} \ddot{\phi} \quad (3.12)$$

$$\frac{\partial^2 \psi}{\partial x_1^2} + \frac{\partial^2 \psi}{\partial x_3^2} = \frac{1}{c_T^2} \ddot{\psi} \quad (3.13)$$

The general solution to equations (3.12) and (3.13), corresponding to plane harmonic wave propagation in positive  $x_1$  direction, may be written as:

$$\phi = \Phi(x_3) e^{i(kx_1 - \omega t)} \quad (3.14)$$

$$\psi = \Psi(x_3) e^{i(kx_1 - \omega t)} \quad (3.15)$$

where  $i = \sqrt{-1}$ . Substitution into (3.12) and (3.13) yields:

$$\frac{\partial^2 \Phi(x_3)}{\partial x_3^2} + \left( \frac{\omega^2}{c_L^2} - k^2 \right) \Phi(x_3) = 0 \quad (3.16)$$

$$\frac{\partial^2 \Psi(x_3)}{\partial x_3^2} + \left( \frac{\omega^2}{c_T^2} - k^2 \right) \Psi(x_3) = 0 \quad (3.17)$$

In applying the appropriate boundary conditions, the solution to equations (3.16) and (3.17), yields displacement and stress fields for a guided wave in an unbounded (in two dimensions) isotropic material, whether it be surface waves or Lamb waves.

### 3.2.1 Propagation in a free isotropic plate

Wave propagation in plates were first studied by Lamb (1917), hence the guided waves in free isotropic plates are called Lamb waves. There are two types of Lamb waves: symmetrical (also called longitudinal or extensional) waves and anti-symmetrical (also called flexural or bending) (Rydén, 2004).

Let's consider a homogeneous, isotropic linear elastic material that occupy the space  $-h/2 < x_3 < h/2$  in  $x_3$ -direction and is unbounded in  $x_1$ - and  $x_2$ -direction, as shown in Figure 3.1. Let's assume lossless interfaces, where only reflections occur, then the Lamb wave may be interpreted as an interference pattern created by multiple reflections and mode conversions of longitudinal waves (P-waves) and vertically polarised shear waves (SV-waves). The resulting modes are a propagating wave in the waveguide direction ( $x_1$ -direction) and a resonance standing wave in the transverse direction ( $x_3$ -direction). The P-wave and SV-wave are coupled, thus wave propagation in  $x_1$  only occurs for certain combinations of angular frequency  $\omega$  and wave number  $k$  that correspond to a given standing wave in  $x_3$  (Auld, 1973; Rydén and Park, 2004). The free isotropic unbounded lossless plate is an idealized, rather than realizable, structure, but it can be useful as a first approximation for various free plates (Auld, 1973).

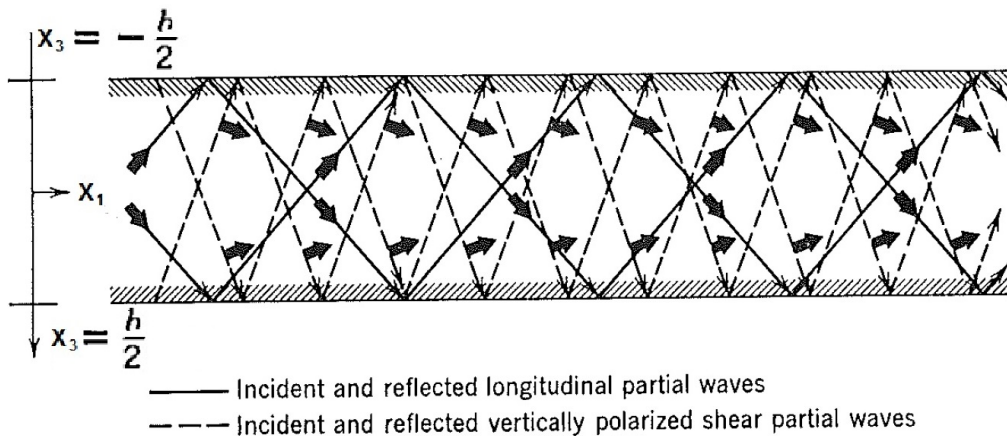


Figure 3.1: A free isotropic plate with infinite extent in  $x_1$ - and  $x_2$ -direction and bounded in  $x_3$ -direction by vacuum, with boundary conditions  $\sigma_{33} = \sigma_{13} = 0$  at  $x_3 = \pm h/2$ . Picture taken from Auld (1973).

Let's consider the relation between the transverse standing wave and the propagating wave, by finding an appropriate solution to the potentials  $\phi$  and

$\psi$  of the displacement field decomposition. A solution to equations (3.16) and (3.17) is obtained by assuming  $\Phi(x_3)$  and  $\Psi(x_3)$  as,

$$\Phi(x_3) = A_1 \sin(px_3) + A_2 \cos(px_3) \quad (3.18)$$

$$\Psi(x_3) = B_1 \sin(qx_3) + B_2 \cos(qx_3) \quad (3.19)$$

where

$$p = \sqrt{\frac{\omega^2}{c_L^2} - k^2}; \quad q = \sqrt{\frac{\omega^2}{c_T^2} - k^2};$$

Substitution into wave equations (3.16) and (3.17) yields:

$$\phi = [A_1 \sin(px_3) + A_2 \cos(px_3)] e^{i(kx_1 - \omega t)} \quad (3.20)$$

$$\psi = [B_1 \sin(qx_3) + B_2 \cos(qx_3)] e^{i(kx_1 - \omega t)} \quad (3.21)$$

Solving the equation system (3.18) and (3.19) with respect to appropriate coefficients  $A_1$ ,  $A_2$ ,  $B_1$ ,  $B_2$ , and the boundary conditions  $\sigma_{33} = \sigma_{13} = 0$  at  $x_3 = \pm h/2$  yields two solutions:

$$\frac{\tan(q\frac{h}{2})}{\tan(p\frac{h}{2})} = -\frac{4k^2 pq}{(q^2 - k^2)^2} \quad (3.22)$$

$$\frac{\tan(q\frac{h}{2})}{\tan(p\frac{h}{2})} = -\frac{(q^2 - k^2)^2}{4k^2 pq} \quad (3.23)$$

These are the *Rayleigh-Lamb* dispersion equations (Achenbach, 1973), for symmetrical (3.22) and anti-symmetrical (3.23) modes, with respect to the center of the plate ( $x_3 = 0$ ). The dispersion equations give the relationship between a given angular frequency  $\omega$  and the wave number  $k$  for a plate with the longitudinal- and transverse phase velocities  $c_L$  and  $c_T$ . However, the dispersion equations are transcendental and no algebraic solution exists, hence they need to be solved numerically. Typically, one solves for the wave number  $k$  by proposing a real and positive  $\omega$  (Achenbach, 1973). For a given angular frequency there exist a finite number of symmetrical and anti-symmetrical Lamb modes. The number of real roots to equation (3.22) is equal to the number of symmetrical modes, and the number of real roots to equation (3.23) is equal to the number of anti-symmetric modes. Each mode differs in phase and group velocities, as well as displacement and stress distribution in the plate, and propagates independently of other modes. The real solutions to (3.22) and (3.23) are shown in Figure 3.3b, where each point

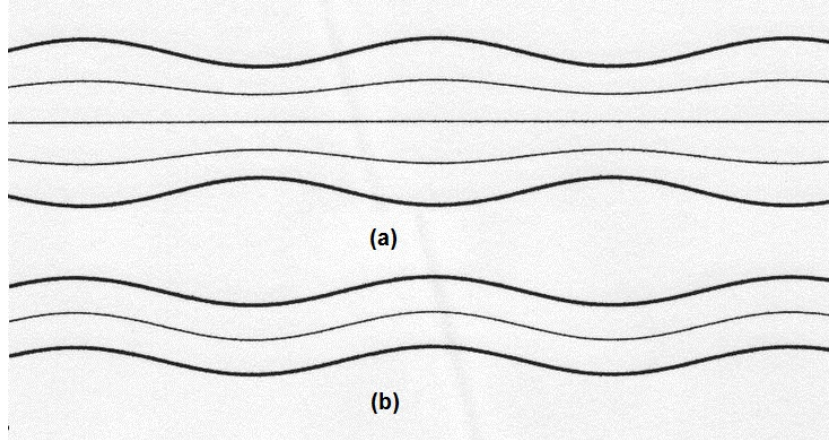


Figure 3.2: (a) Symmetric and (b) Anti-symmetric modes for a free plate.  
Picture taken from Wikimedia Commons, Adrien de Physics, CC BY-SA 3.0

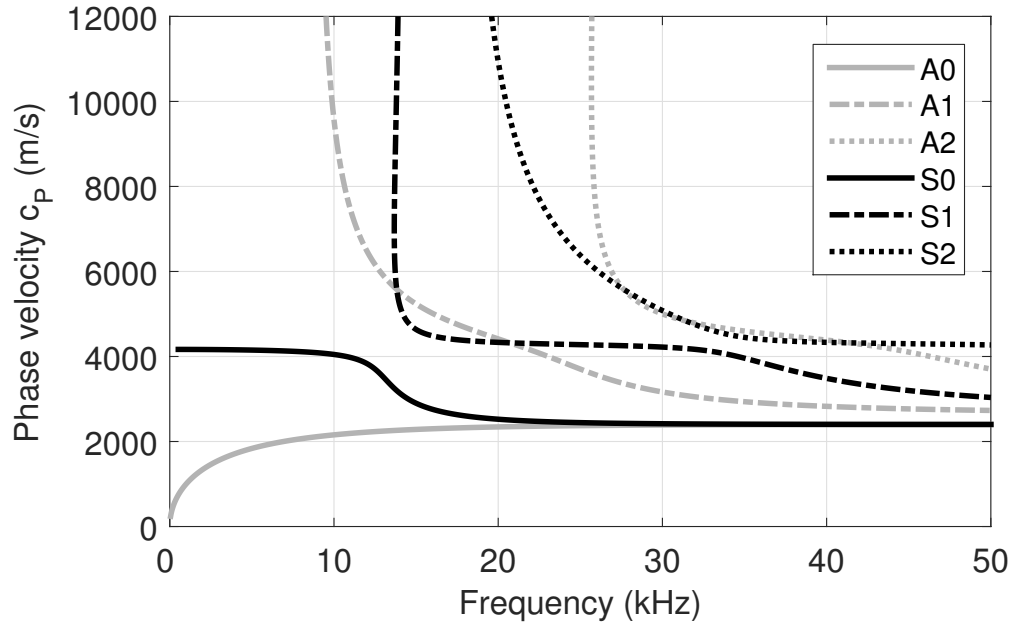
on each curve represents a mode, and the corresponding phase velocities are shown in Figure 3.3a. Note that the conjugated quantities  $c_{ph}-f$  may be expressed in  $k-\omega$  by the relations:  $c_{ph} = \omega/k$  and  $f = \omega/2\pi$ . Let  $fh$  be the frequency-thickness product. For  $fh \rightarrow 0$ , (thus  $\omega h \rightarrow 0$ ) the dispersion equations (3.22) and (3.23) have only one root each. These roots represent the zero symmetrical mode  $S_0$  and the zero anti-symmetrical mode  $A_0$ , respectively. As  $fh$  increases new roots are found. They represent higher symmetrical modes,  $(S_1, S_2, \dots, S_n)$ , and higher anti-symmetrical modes,  $(A_1, A_2, \dots, A_n)$ . The critical frequency-thickness when additional roots appear, is given by the relationship between plate thickness and transverse- and longitudinal wavelength:

$$\left. \begin{array}{l} h = m \lambda_L, \quad m = 1, 2, 3, \dots \\ h = n \frac{\lambda_T}{2}, \quad n = 1, 3, 5, \dots \\ h = n \frac{\lambda_L}{2}, \quad n = 1, 3, 5, \dots \\ h = m \lambda_T, \quad m = 1, 2, 3, \dots \end{array} \right\} \begin{array}{l} \text{for symmetrical modes} \\ \text{for anti-symmetrical modes} \end{array}$$

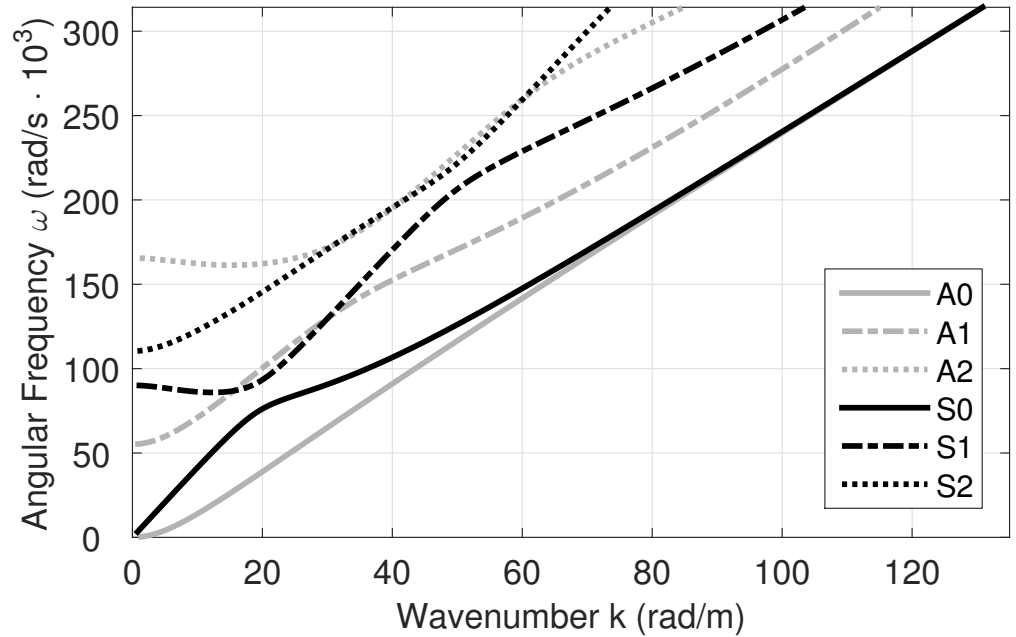
Which may be reformulated as:

$$(fh) = \begin{cases} n \frac{c_L}{2} & n = 1, 2, 3, \dots \\ m \frac{c_T}{2} & m = 1, 2, 3, \dots \end{cases} \quad (3.24)$$

At the critical frequency the phase velocity goes to infinity, as seen in Figure 3.3a. As the zeroth symmetrical mode  $S_0$  approaches zero it converges on



(a)



(b)

Figure 3.3: Six lowest Lamb modes for a homogeneous isotropic linear elastic free plate with infinite extent and symmetrical cross-section. Shear velocity  $c_T = 2635 \text{ m s}^{-1}$ , thickness  $h = 0.15 \text{ m}$  and Poisson's ratio  $\nu = 0.200$

the quasi longitudinal wave velocity,

$$c_{QL} = \sqrt{\frac{E}{\rho(1-\nu^2)}}.$$

As the zeroth anti-symmetrical mode  $A_0$  approaches zero it converge on the bending wave velocity,

$$c_B = \sqrt{\omega h} \left( \sqrt[4]{\frac{E}{3\rho(1-\nu^2)}} \right).$$

As  $fh \rightarrow \infty$ , both  $S_0$  and  $A_0$  converge on the Rayleigh wave velocity. The displacements become localized at the free boundaries, representing two Rayleigh waves propagation, in phase, along the free boundaries ([Viktorov, 1967](#)). For higher modes, the phase velocity converges on the shear wave velocity. The Lamb modes become localized to the interior of the plate, and may not be detected at the boundary. For an in-depth review of displacement distribution in free plates the reader is referred to [Viktorov \(1967\)](#) Chapter II. It is worth noting that pure symmetric and anti-symmetric modes only exist for free plates with a symmetric cross-section, such as in Figure 3.1. However, for unsymmetrical plates there exists in general quasi symmetrical and quasi anti-symmetrical modes ([Ahmad et al., 2013](#)).



# Chapter 4

## SAFE method

Previously, we considered an analytical solution to the Lamb modes for a homogeneous isotropic linear elastic free plate with infinite extent and symmetrical cross-section. However, if we want to consider propagation in a waveguide with an arbitrary cross-section (e.g. with a finite extent or periodic recurrence), anisotropic or damped medium, or arbitrary boundary conditions, this method is insufficient. Therein lies the motivation for applying a numerical scheme, such as the Semi-Analytical Finite Element (SAFE) methods. SAFE has successfully been used to model arbitrary cross-sections, such as rails (Hayashi et al., 2003), periodic structures (Predoi et al., 2007) and composite plates (Ahmad et al., 2013). It has also been shown to be suitable for modelling damped medium (Bartoli et al., 2006), anisotropic medium (Predoi et al., 2007) and leaky medium (Hayashi and Inoue, 2014; Castaings and Lowe, 2008)

In general, the approach when solving the dispersive relation using SAFE is to make a Finite Element (FE) discretisation of the cross-section domain (2D SAFE) or line domain (1D SAFE). In the wave-propagation direction, i.e. normal to the cross-section plane or line, the displacements are modelled using analytical harmonic functions, hence the name semi-analytical. This two dimensional (2D) or one dimensional (1D) discretisation allows computational savings compared to solving a three dimensional (3D) discretisation of the domain - in particular for short wave lengths where a very fine mesh is required (Bartoli et al., 2006).

## 4.1 Mathematical preliminaries

In considering the SAFE methods we'll need to lay down some preliminaries. We'll consider the quadratic eigenvalue problem, the frame work of SAFE and its FE-discretisation. We will in the following derivations consider the 2D discretisation. However, the 1D SAFE is easily derived, as a special case of the 2D SAFE.

### 4.1.1 Quadratic Eigenvalue Problems

Quadratic Eigenvalue Problems (QEP) occurs extensively within dynamic analysis of mechanical systems ([Tisseur and Meerberg, 2001](#)). Let's consider the linear second order PDE,

$$M\ddot{q} + C\dot{q} + Kq = f, \quad (4.1)$$

where  $M, C, K$  are  $n \times n$  (complex) matrices. The solution may be expressed as an eigensolution of the corresponding QEP, where the eigenvalues and eigenvectors must satisfy,

$$(\lambda^2 M + \lambda C + K)x = 0, \quad y^* (\lambda^2 M + \lambda C + K) = 0; \quad (4.2)$$

where  $x, y$  are the so called right and left eigenvector, respectively, to the corresponding eigenvalue  $\lambda$ . QEP differ from standard eigenvalue problems (SEP),

$$Ax = \lambda x,$$

and the general eigenvalue problem (GEP),

$$Ax = \lambda Bx,$$

in that the QEP has  $2n$  eigenvalues, and  $2n$  right and  $2n$  left eigenvectors, rather than  $n$  eigenvalues ([Tisseur and Meerberg, 2001](#)).

Let's consider the solution to equation (4.2). Let  $Q(\lambda)$ , called the  $\lambda$ -matrix, be an  $n \times n$  matrix polynomial of degree 2,

$$Q(\lambda) = \lambda^2 M + \lambda C + K, \quad (4.3)$$

or in other words, the coefficients of  $Q(\lambda)$  are quadratic polynomials in  $\lambda$ . Let  $\Lambda(Q)$  be the spectrum of  $Q(\lambda)$ ,

$$\Lambda(Q) = \{\lambda \in \mathbb{C} : \det Q(\lambda) = 0\},$$

or in other words, the set of eigenvalues of  $Q(\lambda)$ . The set contains  $2n$  distinct eigenvalues, that may be real or complex (Tisseur and Meerberg, 2001). However, there only exists a set of  $n$  linearly independent eigenvectors (Gohberg et al., 1982). If the coefficient matrices are real, the spectrum  $\Lambda(Q)$  is symmetric with respect to the real axis of the complex plane. Therefore, eigenvalues are either real or come in complex conjugate pairs  $(\lambda, \bar{\lambda})$ . Real coefficient matrices correspond to an undamped system. Complex coefficient matrices corresponds to a damped system (Tisseur and Meerberg, 2001).

The QEP may be linearised, i.e. reduced to a first-order equation, analogously to how the underlying PDE may be linearised. Let  $q_0 = q$  and  $q_1 = \dot{q}_0$ , so that equation (4.1) may be rewritten as an equivalent system of  $2n$  unknowns,

$$\begin{aligned} M\dot{q}_1 + Cq_1 + Kq_0 &= f, \\ q_1 &= \dot{q}_0, \end{aligned}$$

Similarly, the substitution  $u = \lambda x$  into equation (4.2), yields a linearisation in  $2n$  unknowns, of the first companion form,

$$L1 : \quad \begin{cases} \lambda Mu + Cu + Kx &= 0, \\ u &= \alpha \lambda x, \end{cases}$$

where  $Q(\lambda)$  reduces to the corresponding GEP  $(A - \lambda B)$ ,

$$\left( \begin{bmatrix} 0 & \alpha I \\ -K & -C \end{bmatrix} - \lambda \begin{bmatrix} \alpha I & 0 \\ 0 & M \end{bmatrix} \right) \begin{bmatrix} x \\ u \end{bmatrix} = 0, \quad (4.4)$$

or the second companion form,

$$L2 : \quad \begin{cases} \lambda Mu + \lambda Cx + Kx &= 0, \\ u &= \alpha \lambda x, \end{cases}$$

with the corresponding GEP,

$$\left( \begin{bmatrix} -K & 0 \\ 0 & \alpha I \end{bmatrix} - \lambda \begin{bmatrix} C & M \\ \alpha I & 0 \end{bmatrix} \right) \begin{bmatrix} x \\ u \end{bmatrix} = 0, \quad (4.5)$$

where  $I$  is the identity matrix and  $\alpha$  a scalar. These are the more commonly used linearisations. However, any  $2n \times 2n$  linear GEP  $(A - \lambda B)$  that fullfills,

$$\begin{bmatrix} Q(\lambda) & 0 \\ 0 & I \end{bmatrix} = E(\lambda)(A - \lambda B)F(\lambda), \quad (4.6)$$

where  $E(\lambda)$  and  $F(\lambda)$  are  $2n \times 2n$   $\lambda$ -matrices with constant non-zero determinants, is a linearisation of  $Q(\lambda)$ . The eigenvalues of  $Q(\lambda)$  and  $A - \lambda B$  coincide. However, the linearisation is not unique, and care need to be taken to the form of linearisation if one wants to keep symmetry or other structural properties of  $Q(\lambda)$  ([Tisseur and Meerberg, 2001](#)).

Large QEPs are typically solved using iterative methods, where increasingly accurate approximations are found in sequences of subspaces  $\{K_k \in \mathbb{C}^{n \times k} : k \leq n\}$  to  $\{Q(\lambda) \in \mathbb{C}^{n \times n}\}$ . A numerical scheme called the *implicitly restarted Arnoldi method*, is provided by the ARPACK software, and is implemented in commercial softwares such as Matlab ([Tisseur and Meerberg, 2001](#)) and Comsol ([COMSOL, 2012](#)).

### 4.1.2 SAFE mathematical framework

Let's consider a wave guide. Let the wave propagate along the  $x_3$ -axis, with the wave number  $k$  and angular frequency  $\omega$ . The waveguide cross-section lies in the  $x_1$ - $x_2$  plane. Let's consider the displacement equations of motion:

$$C_{ijkl} \frac{\partial^2 u_k}{\partial x_i \partial x_j} - \rho \frac{\partial^2 u_i}{\partial t^2} = 0. \quad (4.7)$$

Propagation in the  $x_3$ -direction implies that the propagation direction unit vector  $\vec{n}_m = (0, 0, 1)$ . Let the amplitude  $U_i$  of the displacement field be independent of the direction of propagation, such that  $U_i = U_i(x_1, x_2)$ . One may propose a general solution to equation (4.7) for the wave guide such that,

$$u_i(x_1, x_2, x_3, t) = U_i(x_1, x_2) e^{I(kx_3 - \omega t)}, \quad i \in \{1, 2, 3\}, \quad (4.8)$$

where  $I = \sqrt{-1}$ . Herein lies the separation of the cross-section plane domain from the out-of-plane wave propagation domain, which now is described by the analytical function  $e^{I(kx_3 - \omega t)}$ . The assumption in making the separation, is that the cross-section and material properties remains constant along  $x_3$ . The 1D SAFE is a special case of 2D SAFE where the displacement amplitude is only dependent on the position along a line domain, thus  $U_i = U_i(x_1)$ . This approach is analogous to the approach in Section 3.2.1 where the dispersion relation for an isotropic homogeneous linear elastic plate was derived.

Let's consider the derivatives of the displacement field,

$$\frac{\partial u_i}{\partial x_1} = \frac{\partial U_i}{\partial x_1} e^{I(kx_3 - \omega t)}, \quad (4.9)$$

$$\frac{\partial u_i}{\partial x_2} = \frac{\partial U_i}{\partial x_2} e^{I(kx_3 - \omega t)}, \quad (4.10)$$

$$\frac{\partial u_i}{\partial x_3} = I k U_i e^{I(kx_3 - \omega t)}, \quad (4.11)$$

$$\frac{\partial u_i}{\partial t} = -I \omega U_i e^{I(kx_3 - \omega t)}. \quad (4.12)$$

Substitution of (4.12) into equation (4.7) yields:

$$C_{ijkl} \frac{\partial^2 u_k}{\partial x_l \partial x_j} + \rho \omega^2 u_i = 0, \quad i, j, k, l \in \{1, 2, 3\}. \quad (4.13)$$

Substitution of equations (4.9)-(4.11) into equation (4.13) and explicitly writing out the summation of the derivatives in  $x_3$ , i.e. when indices  $l = 3$  and  $j = 3$ , yields,

$$C_{ijkl} \frac{\partial^2 u_k}{\partial x_l \partial x_j} + I k C_{i3kl} \frac{\partial u_k}{\partial x_l} + I k C_{ijk3} \frac{\partial u_k}{\partial x_j} - k^2 C_{i3k3} u_k + \rho \omega^2 u_i = 0, \quad (4.14)$$

$$i, k \in \{1, 2, 3\}, \quad j, l \in \{1, 2\}.$$

Through division with  $e^{I(kx_3 - \omega t)}$  and appropriate renaming of dummy indices, equation (4.14) may be reformulated as,

$$C_{ijkl} \frac{\partial^2 U_k}{\partial x_l \partial x_j} + I k (C_{i3kj} + C_{ijk3}) \frac{\partial U_k}{\partial x_j} - k^2 C_{i3k3} U_k + \rho \omega^2 \delta_{ik} U_k = 0; \quad (4.15)$$

$$i, k \in \{1, 2, 3\}, \quad j, l \in \{1, 2\}.$$

The *natural* or *Neumann boundary conditions* enter as the traction vector  $t_i$  on the boundary  $\delta\Omega$ ,

$$t_i = \sigma_{ij} n_j = C_{ijkl} \frac{\partial U_k}{\partial x_l} n_j, \quad i, j, k, l \in \{1, 2, 3\}, \quad (4.16)$$

where  $n_j$  is the outward unit normal vector to the boundary  $\delta\Omega$ .

The solution to equation (4.15) yields the dispersion relation. To find appropriate roots to (4.15) we want to recast it as a QEP, in the parameters  $k$  and  $\omega$ . To achieve this we need to find the derivatives of  $U_k$ . Consequently,

a numerical approximation of the displacement field must be made. Herein lies the motivation to apply an FE-discretisation. Thereby, the derivatives of  $U_k$  may be related to the derivatives of the approximating shape functions. Which, allows for the equivalent *weak formulation* to the *strong formulation* in (4.15) to be made. Let's go ahead and consider an FE-discretisation.

### 4.1.3 FE-discretisation

A dynamic system may be described by *Hamilton's principle*. Hence, we'll derive the equations of motion yet again, but now from the starting point of energy, and through the use of *calculus of variation*. The aim is to derive an FE-approximation that allows the reformulation of equation (4.15) into a QEP. Let the *Hamiltonian*  $H$  be,

$$H = T + V, \quad (4.17)$$

where  $T$  is the kinetic energy,

$$T = \frac{1}{2} \int_{\Omega} \dot{u}^T \rho \dot{u} \, d\Omega, \quad (4.18)$$

and  $V$  some potential function that is velocity independent. In other words,  $V$  is independent of frictional and viscous damping. Then the potential function  $V$  reduces to the *strain energy function*  $W$ ,

$$W = \frac{1}{2} \int_{\Omega} \varepsilon^T C \varepsilon \, d\Omega. \quad (4.19)$$

For a free system, i.e. where no external traction or body forces are applied, the variation of the Hamiltonian is,

$$\delta H = \int_{t_1}^{t_2} \delta (W - T) \, dt = 0. \quad (4.20)$$

This is the conservative formulation of Hamilton's principle, i.e. a system where no energy is dissipated. To account for dissipation a non-conservative form of Hamilton's principle should be used (Bartoli et al., 2006). However, it's been shown that a conservative formulation may be used to describe a non-conservative motion due to dissipation, if the strain energy distribution over the cross-section is not significantly changed by increasing levels of damping (Shorter, 2004). By introducing a complex valued elasticity tensor  $C_{ijkl}$ ; an estimate of the dissipation (damping) is given by the resulting imaginary part of the wave number  $k$  (Bartoli et al., 2006).

Equation (4.20) may through integration by parts of the kinetic energy term be formulated as,

$$\delta H = \int_{t_1}^{t_2} \left[ \int_{\Omega} \delta(\varepsilon^T) C \varepsilon d\Omega + \int_{\Omega} (\dot{u}^T) \rho \dot{u} d\Omega \right] dt = 0. \quad (4.21)$$

Let the strain  $\varepsilon$  be,

$$\varepsilon = \left[ L_1 \frac{\partial}{\partial x_1} + L_2 \frac{\partial}{\partial x_2} + L_3 \frac{\partial}{\partial x_3} \right] u, \quad (4.22)$$

where

$$L_1 = \begin{bmatrix} 1 & 0 & 0 \\ 0 & 0 & 0 \\ 0 & 0 & 0 \\ 0 & 0 & 0 \\ 0 & 0 & 1 \\ 0 & 1 & 0 \end{bmatrix}, \quad L_2 = \begin{bmatrix} 0 & 0 & 0 \\ 0 & 1 & 0 \\ 0 & 0 & 0 \\ 0 & 0 & 1 \\ 0 & 0 & 0 \\ 1 & 0 & 0 \end{bmatrix}, \quad L_3 = \begin{bmatrix} 0 & 0 & 0 \\ 0 & 0 & 0 \\ 0 & 0 & 1 \\ 0 & 1 & 0 \\ 1 & 0 & 0 \\ 0 & 0 & 0 \end{bmatrix}.$$

Let FE-discretisation in the element domain  $\Omega_e$ , be dependent of  $n$  nodal points, shape functions  $N_j^{(e)}(x_1, x_2)$  and the element nodal displacements  $U_j^{(e)}(x_1, x_2) = (U_{1j}, U_{2j}, U_{3j})$ , where  $\{j \in \mathbb{N}_1 : j \leq n\}$ . Then the corresponding FE-approximation of equation (4.8) is,

$$u^{(e)}(x_1, x_2, x_3, t) = \begin{bmatrix} \sum_{j=1}^n N_j^{(e)}(x_1, x_2) U_{1j} \\ \sum_{j=1}^n N_j^{(e)}(x_1, x_2) U_{2j} \\ \sum_{j=1}^n N_j^{(e)}(x_1, x_2) U_{3j} \end{bmatrix} e^{I(kx_3 - \omega t)} = N(x_1, x_2) q^{(e)} e^{I(kx_3 - \omega t)}, \quad (4.23)$$

where

$$N(x_1, x_2) = \begin{bmatrix} N_1^{(e)} & N_2^{(e)} & \ddots & N_j^{(e)} \\ N_1^{(e)} & N_2^{(e)} & \ddots & N_j^{(e)} \\ N_1^{(e)} & N_2^{(e)} & \ddots & N_j^{(e)} \end{bmatrix},$$

$$q^{(e)} = [U_{11}, U_{21}, U_{31}, U_{12}, U_{22}, U_{32}, \dots, \dots, \dots, U_{1n}, U_{2n}, U_{3n}]^T.$$

The element strain vector  $\varepsilon^{(e)}$ , is obtained by substitution of (4.23) into equation (4.22),

$$\varepsilon^{(e)} = (B_1 + \text{Ik} B_2) q^{(e)} e^{\text{I}(kx_3 - \omega t)}, \quad (4.24)$$

where

$$\begin{aligned} B_1 &= L_1 \frac{\partial N}{\partial x_1} + L_2 \frac{\partial N}{\partial x_2}, \\ B_2 &= L_3 N. \end{aligned}$$

Hence, the first term in equation (4.21) may, after some manipulations, be written as,

$$\begin{aligned} &\int_{\Omega_e} \delta \left( \varepsilon^{(e)\text{T}} \right) C \varepsilon^{(e)} d\Omega_e \\ &= \delta q^{(e)\text{T}} \left( \int_{\Omega_e} [B_1^T C B_1 - \text{Ik} B_2^T C B_1 + \text{Ik} B_1^T C B_2 + k^2 B_2^T C B_2] d\Omega_e \right) q^{(e)}, \end{aligned} \quad (4.25)$$

and the second term may be written as,

$$\int_{\Omega_e} \left( \dot{u}^{(e)\text{T}} \right) \rho \dot{u}^{(e)} d\Omega_e = \delta q^{(e)\text{T}} \left( -\omega^2 \int_{\Omega_e} N^T \rho N d\Omega \right) q^{(e)}. \quad (4.26)$$

For a comprehensive derivation of the expressions the reader is referred to (Bartoli et al., 2006). Substitution of (4.25) and (4.26) into equation (4.21), and application of the standard finite element assembly operator  $\cup$  yields,

$$\int_{t_1}^{t_2} \left( \bigcup_{e=1}^{n_{el}} \delta q^{(e)\text{T}} \left[ K_1^{(e)} + \text{Ik} K_2^{(e)} + k^2 K_3^{(e)} - \omega^2 M^{(e)} \right] q^{(e)} \right) dt = 0 \quad (4.27)$$

where

$$\begin{aligned} K_1^{(e)} &= \int_{\Omega_e} B_1^T C B_1 d\Omega, & K_2^{(e)} &= \int_{\Omega_e} (-B_2^T C B_1 + B_1^T C B_2) d\Omega, \\ K_3^{(e)} &= \int_{\Omega_e} B_2^T C B_2 d\Omega, & M^{(e)} &= \int_{\Omega_e} N^T \rho N d\Omega, \end{aligned}$$

The variations of the displacements  $\delta q^{(e)}$  are arbitrary. Consequently, in applying the assembly operator over all elements yields the global homogeneous system,

$$\int_{t_1}^{t_2} \left( [K_1 + \text{Ik} K_2 + k^2 K_3 - \omega^2 M] q \right) dt = 0, \quad (4.28)$$

with its equivalent eigenvalue form,

$$[K_1 + IkK_2 + k^2 K_3 - \omega^2 M] q = 0. \quad (4.29)$$

where  $q$  is the global nodal displacement vector.

In discretising the cross-section domain, the strong formulation of (4.15) may be formulated as a similar matrix formulation (4.29). The derivatives of the displacements in (4.15) are replaced by the global nodal displacement vector  $q$ , with  $n$  degrees-of-freedom. Obviously, equation (4.29) is a quadratic eigenvalue problem in wavenumber  $k$ . However, it differs from the form given in (4.2), in that it's a twin parameter problem in wavenumber  $k$  and angular frequency  $\omega$ . An eigensolution may be found by proposing a real positive  $\omega$  and solving for the wavenumber  $k$ , as well as proposing a real or complex wavenumber and solving for the angular frequency  $\omega$ . Typically, one proposes an angular frequency  $\omega$  and solves for the wavenumber  $k = k(\omega)$ , since it allows for the study of both propagating and non-propagating waves as well as damped medium (Bartoli et al., 2006). Rather than implementing the FE-formulation given in (4.29) we'll use the commercial finite element program Comsol. However, for clarity, it's been shown that it is reasonable to pursue a cross-sectional discretisation to find the solution to the dispersion relation.

#### 4.1.4 Solutions to undamped medium

For an undamped medium the elasticity tensor  $C_{ijkl}$  is real valued. Hence, the eigenvalues are real or come in pairs  $(\lambda, \bar{\lambda})$  (Tisseur and Meerberg, 2001). Real wave numbers correspond to propagating modes in  $x_3$  direction. Complex wave numbers with both a real and imaginary part correspond to evanescent waves with decaying amplitudes in  $x_3$ -direction. Purely imaginary wavenumbers correspond to non-oscillating evanescent waves in  $x_3$  direction. The phase velocity  $c_{ph}$  for the lamb wave is computed for a given angular frequency  $\omega$  by division with corresponding real valued wavenumbers,

$$c_{ph} = \omega/k_{real}.$$

For undamped medium the cut-off frequency may be computed by letting  $k = 0$  and solving for  $\omega$  (Bartoli et al., 2006). Whereby, Equation (4.29) reduces to,

$$[K_1 + \omega^2 M] q = 0. \quad (4.30)$$

### 4.1.5 Solutions to damped medium

For a damped medium the elasticity tensor  $C_{ijkl}$  is complex valued, see Section 2.4, and, thus, all eigenvectors and eigenvalues are complex valued. Hence, there is no numerical distinction between propagating and evanescent waves (Bartoli et al., 2006). Neither are the eigenvalues, i.e. wavenumbers, to the dispersion relation symmetric around the real axis in the complex plane. In other words the wavenumbers does not have complex conjugate roots. The concept of cut-off frequency doesn't have any meaning for damped medium since  $k = 0$  is not a root to (4.29) for  $\omega > 0$  (Rose, 1999). If a Kelvin-Voigt model is used the elasticity tensor need to be updated for every  $\omega$ . For a hysteretic model the elasticity tensor need to be computed only once (Bartoli et al., 2006).

## 4.2 Comsol Multiphysics

Comsol Multiphysics is a commercial finite element software. It allows one to specify, and solve, user-defined *partial differential equations* in its PDE-mode. Let  $\Omega$  be the computational domain (in one, two or three dimensions) with the domain boundary  $d\Omega$ . Let  $\mathbf{n}$  be an outward unit normal vector on  $d\Omega$ . Let  $\mathbf{u}$  be a  $n$ -dimensional vector containing the dependent (unknown) variables, such that  $\mathbf{u} = (u_1, u_2, \dots, u_n)$  on the computational domain. For a stationary problem the input formalism for Comsol's *coefficient form PDE interface* is,

$$\nabla \cdot (c\nabla u + \alpha u - \gamma) - \beta \nabla u - au - \lambda d_a u = 0 \quad \text{in } \Omega, \quad (4.31)$$

$$n \cdot (c\nabla u + \alpha u - \gamma) - qu = g - h^T \mu \quad \text{in } d\Omega, \quad (4.32)$$

$$hu = r \quad \text{in } d\Omega, \quad (4.33)$$

where equation (4.31) is the general PDE, which must be satisfied in  $\Omega$ . Equations (4.32) and (4.33) is the generalized Neumann boundary condition and Dirichlet boundary condition, respectively. Remaining coefficients are user specified coefficient matrices, that may be arbitrary functions - including functions in  $\mathbf{u}$  and its derivatives or constants. Coefficient matrices can be both real and complex valued (COMSOL, 2012).

A reformulation of the SAFE method, as given in equation (4.15),

$$C_{ijkl} \frac{\partial^2 U_k}{\partial x_l \partial x_j} + ik(C_{i3kj} + C_{ijk3}) \frac{\partial U_k}{\partial x_j} - k^2 C_{i3k3} U_k + \rho \omega^2 \delta_{ik} U_k = 0; \\ i, k \in \{1, 2, 3\}, \quad j, l \in \{1, 2\}.$$

into the Comsol formalism was proposed by Predoi et al. (2007). If  $\gamma = 0$  equation (4.15) may be expressed in (4.31) as,

$$c \frac{\partial^2 U_k}{\partial x_l \partial x_j} + (\alpha - \beta) \frac{\partial U_k}{\partial x_j} - a U_k + \lambda d_a U_k = 0; \quad (4.34)$$

and similarly, the traction (4.16) may be expressed in (4.32). A first companion form linearisation in  $2n$  unknowns is made,

$$M V_k = M \lambda U_k, \quad k \in \{1, 2, 3\}. \quad (4.35)$$

where  $\lambda$  correspond to the wavenumber  $k$ , as opposed to indices  $k$ . Hence, the dependent vector  $U = [U_1, U_2, U_3, V_1, V_2, V_3]^T$ . The coefficient matrices are thus given as,

$$\begin{aligned} d_a &= \begin{bmatrix} \mathbf{0} & \mathbf{D} \\ \mathbf{M} & \mathbf{0} \end{bmatrix}; & c &= \begin{bmatrix} \mathbf{C} & \mathbf{0} \\ \mathbf{0} & \mathbf{0} \end{bmatrix}; & \alpha &= \begin{bmatrix} \mathbf{0} & i\mathbf{A} \\ \mathbf{0} & \mathbf{0} \end{bmatrix}; \\ \beta &= \begin{bmatrix} \mathbf{0} & -i\mathbf{B} \\ \mathbf{0} & \mathbf{0} \end{bmatrix}; & a &= \begin{bmatrix} \mathbf{M} & \mathbf{0} \\ \mathbf{0} & \mathbf{M} \end{bmatrix}; & \gamma &= [\mathbf{0}] \end{aligned}$$

where  $i = \sqrt{-1}$  and,

$$\begin{aligned} \mathbf{A} &= \begin{bmatrix} \begin{bmatrix} C_{15} \\ C_{65} \end{bmatrix} & \begin{bmatrix} C_{14} \\ C_{64} \end{bmatrix} & \begin{bmatrix} C_{13} \\ C_{63} \end{bmatrix} \\ \begin{bmatrix} C_{65} \\ C_{25} \end{bmatrix} & \begin{bmatrix} C_{64} \\ C_{24} \end{bmatrix} & \begin{bmatrix} C_{63} \\ C_{23} \end{bmatrix} \\ \begin{bmatrix} C_{55} \\ C_{45} \end{bmatrix} & \begin{bmatrix} C_{54} \\ C_{44} \end{bmatrix} & \begin{bmatrix} C_{53} \\ C_{43} \end{bmatrix} \end{bmatrix}, \quad \mathbf{B} = \begin{bmatrix} \begin{bmatrix} C_{51} \\ C_{56} \end{bmatrix} & \begin{bmatrix} C_{56} \\ C_{52} \end{bmatrix} & \begin{bmatrix} C_{55} \\ C_{54} \end{bmatrix} \\ \begin{bmatrix} C_{41} \\ C_{46} \end{bmatrix} & \begin{bmatrix} C_{46} \\ C_{42} \end{bmatrix} & \begin{bmatrix} C_{45} \\ C_{44} \end{bmatrix} \\ \begin{bmatrix} C_{31} \\ C_{36} \end{bmatrix} & \begin{bmatrix} C_{36} \\ C_{32} \end{bmatrix} & \begin{bmatrix} C_{35} \\ C_{34} \end{bmatrix} \end{bmatrix}, \\ \mathbf{C} &= \begin{bmatrix} \begin{bmatrix} C_{11} & C_{16} \end{bmatrix} & \begin{bmatrix} C_{16} & C_{12} \end{bmatrix} & \begin{bmatrix} C_{15} & C_{14} \end{bmatrix} \\ \begin{bmatrix} C_{61} & C_{66} \end{bmatrix} & \begin{bmatrix} C_{66} & C_{62} \end{bmatrix} & \begin{bmatrix} C_{65} & C_{64} \end{bmatrix} \\ \begin{bmatrix} C_{61} & C_{66} \end{bmatrix} & \begin{bmatrix} C_{66} & C_{62} \end{bmatrix} & \begin{bmatrix} C_{65} & C_{64} \end{bmatrix} \\ \begin{bmatrix} C_{21} & C_{26} \end{bmatrix} & \begin{bmatrix} C_{26} & C_{22} \end{bmatrix} & \begin{bmatrix} C_{25} & C_{24} \end{bmatrix} \\ \begin{bmatrix} C_{51} & C_{56} \end{bmatrix} & \begin{bmatrix} C_{56} & C_{52} \end{bmatrix} & \begin{bmatrix} C_{55} & C_{54} \end{bmatrix} \\ \begin{bmatrix} C_{41} & C_{46} \end{bmatrix} & \begin{bmatrix} C_{46} & C_{42} \end{bmatrix} & \begin{bmatrix} C_{45} & C_{44} \end{bmatrix} \end{bmatrix}, \quad \mathbf{D} = \begin{bmatrix} -C_{55} & -C_{54} & -C_{53} \\ -C_{45} & -C_{44} & -C_{43} \\ -C_{35} & -C_{35} & -C_{33} \end{bmatrix}, \\ \mathbf{M} &= \begin{bmatrix} -\rho\omega^2 & 0 & 0 \\ 0 & -\rho\omega^2 & 0 \\ 0 & 0 & -\rho\omega^2 \end{bmatrix}, \end{aligned}$$

where  $C_{ij}$  is the contracted notation for the elasticity tensor.



Chapter **5**

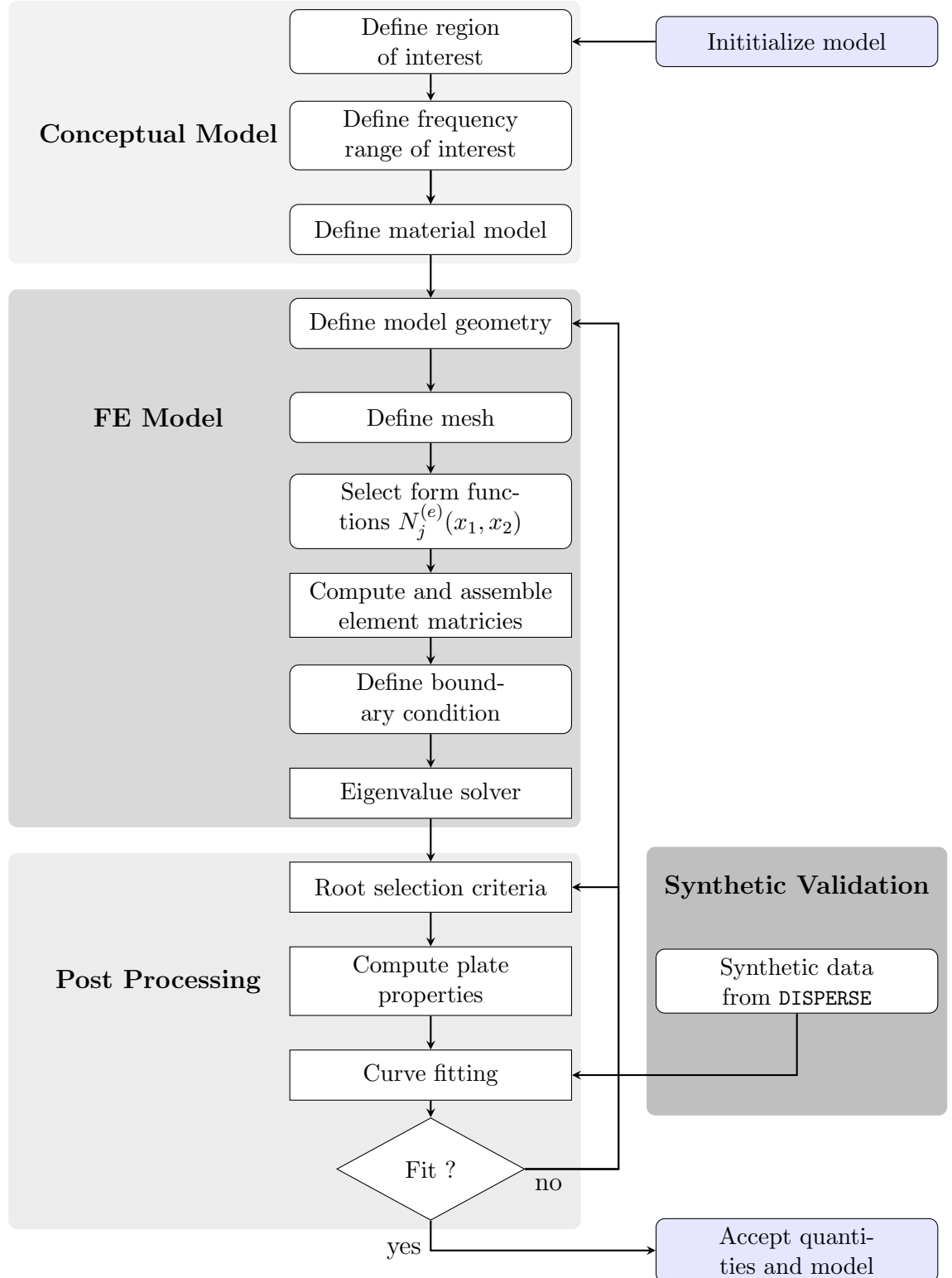
# Case Studies

In this chapter we'll consider some applications of SAFE and guided waves that are of interest in civil engineering. First, we'll consider the minimal requirements of a SAFE discretisation. Namely, that it yields the same solution for a continuous homogeneous isotropic linear elastic free plate as the analytical solution considered in Section 3.2.1. Secondly, we'll consider extended properties of guided wave propagation, such as energy velocity and excitability. Thirdly, we'll consider the effects of proportional damping. Fourthly, we'll consider the effects of a stiffness gradient on zero group velocity modes and, finally, the leaky characteristics of a multi-layered half-space (e.g. pavement structure).

## 5.1 Modelling process

The modelling process, see Figure 5.1, is divided into three parts. First, (1) defining the conceptual model of the structure. This includes defining the region and frequency range of interest and adopting a material model for the structure. Secondly, (2) making an FE model of the conceptual model, and solving the resulting eigenvalue problem. Thirdly, (3) the acquired solution is post-processed to extract relevant information. Physically meaningful roots are selected and spurious roots are discarded. Furthermore, wave number roots may be identified as propagating, oscillating evanescent or non-oscillating evanescent. The criteria whereby roots are selected are not obvious. To the author's knowledge no stringent method or criteria has been proposed in the SAFE literature. Instead, an heuristic approach is adopted based on the root's complex argument and time-averaged power flow. However, like other heuristic approaches it is problem specific, and, hence, does

Figure 5.1: Modelling process flowchart



not lend itself to be generalized. From the selected roots and corresponding eigenvectors the phase velocity, energy velocity, attenuation and excitability may be computed. To determine the quality of the solution it needs to be validated.

In practical inspection systems the model data is validated against experimental data. In this thesis the validation is made against synthetic data from the matrix method software **DISPERSE**. Hence, the synthetic data from **DISPERSE** may be regarded as reference datum or *true* solution. Consequently, the notion of a *correct* SAFE solution is always contingent on the matrix method solution, and is, thus, not a statement about the capability of making a correct prediction with respect to an actual measurable plate.

The validation is made through curve fitting of SAFE data to the synthetic data. If there is a poor fit between SAFE and **DISPERSE** solutions the selection criteria or FE model (e.g. element size, integration rules, size of absorbing region) is updated. Iteratively, the model and selection criteria is refined until an appropriate solution for comparison is achieved.

## 5.2 Solving for a continuous homogeneous isotropic linear elastic free plate

Both a 1D SAFE and a 2D SAFE discretisation will be considered for a continuous homogeneous isotropic linear elastic free plate. The properties of the plate are given by Table 5.1. The material properties given in Table 5.1 belong within the range of values characteristic to concrete (Rydén, 2004). No damping is introduced into the system, thus the elasticity tensor  $C_{ijkl}$  is real valued.

Table 5.1: Plate parameters

| $c_T$ (m/s) | $c_L$ (m/s) | $\rho$ (kg/m <sup>3</sup> ) | $E$ (GPa) | $\nu$ (-) | Damping | Thickness (m) |
|-------------|-------------|-----------------------------|-----------|-----------|---------|---------------|
| 2635.23     | 4303.31     | 2400                        | 40        | 0.200     | None    | 0.15          |

### 5.2.1 2D SAFE Implementation

The cross-section is modelled using a rectangle occupying a region  $\{\Omega \in \mathbb{D}^2 : 0 \leq x_1 \leq h, -h/8 \leq x_2 \leq h/8\}$ , where  $h$  is the cross-section height,

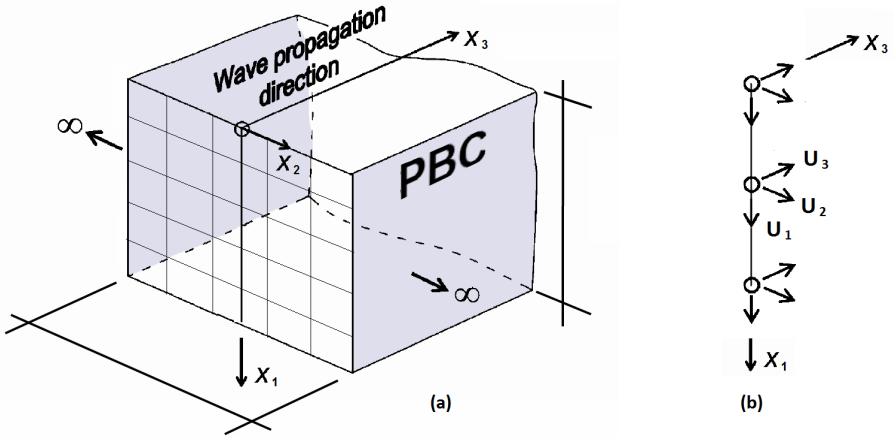


Figure 5.2: (a) 2D SAFE model with meshed cross-section in the  $x_1$ - $x_2$ -plane and periodic boundary (PBC) conditions representing infinite extent in horizontal direction. (b) 1D SAFE representation of the same cross-section as a line domain. Picture taken from [Bartoli et al. \(2006\)](#).

see Figure 5.2a. Since the height is constant in  $x_2$ , the primitive cell of the periodic structure is not defined. Hence, the cross-section width may be arbitrarily chosen. The upper and lower boundaries are assumed to be stress-free. On the vertical boundaries the Dirichlet boundary conditions (4.33) and Neumann boundary conditions (4.32) are given as *periodic boundary conditions*. Continuity is assured, by

$$u|_{x_2=-h/8} = u|_{x_2=h/8},$$

$$\nabla u|_{x_2=-h/8} = \nabla u|_{x_2=h/8},$$

for both displacements and stresses, without prescribing a specific value. The domain is partitioned into 2636 quadratic four-sided elements. The dispersion relations are solved for 350 frequencies between 100 Hz and 35 kHz. The eigenvalue search is truncated at 80 wave number roots, with a centre of root search around  $k = f/(2\pi c_T)$ .

Since the system is undamped, the coefficient matrices are real-valued. Hence, propagating modes may be identified by selecting real valued roots, see the discussion in Section 4.1.4. A root may be classified as a symmetric or anti-symmetric mode by comparing the displacement normal to the plate surface at the boundaries. In other words, the classification is made by comparing SAFE mode shapes with analytical mode shapes, see Figure 3.2. Horizontally

polarized shear modes SH are classified by having predominant displacements in  $x_2$ , i.e. the direction normal to a plane defined by the thickness direction ( $x_1$ ) and wave propagation direction ( $x_3$ ).

### 5.2.2 1D SAFE Implementation

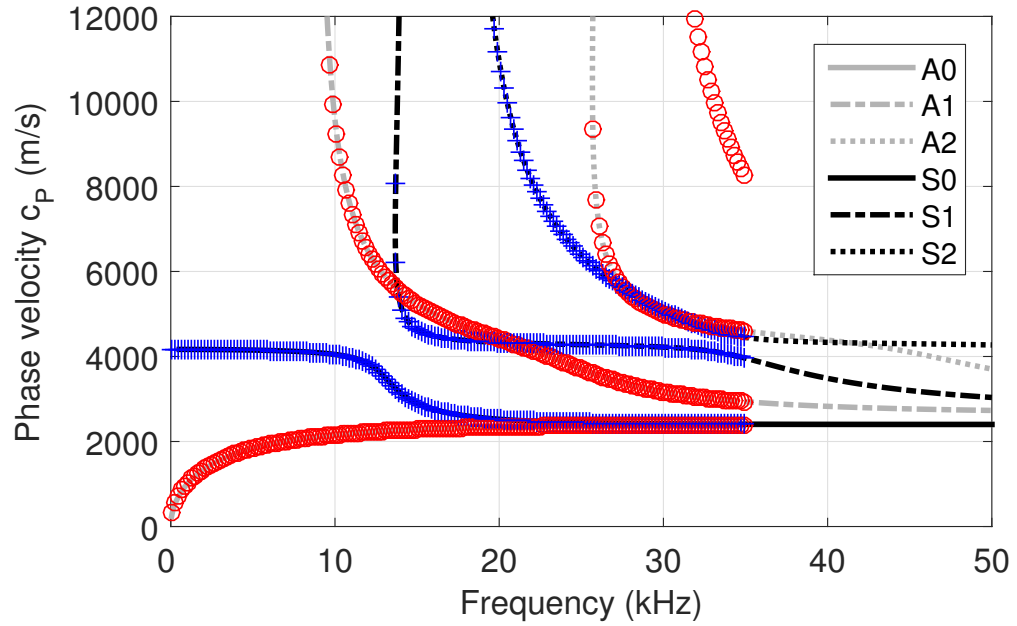
Since the width of the model cross-section may be chosen arbitrarily, we may consider the limit where the width goes to zero. Consequently, the cross-section degenerates to a line domain, see Figure 5.2b. Hence, the computational domain reduces to  $\{\Omega \in \mathbb{D}^1 : 0 \leq x_1 \leq h\}$ . No periodic boundary conditions are needed since the left hand and right hand boundary coincide in the line domain, i.e. continuity is assured by default. The upper and lower surface nodes are assumed stress free. The domain is partitioned into 106 quadratic line elements. The dispersion relations are solved for 350 frequencies between 100 Hz and 35 kHz. The eigenvalue search is truncated at 80 wave number roots, with a centre of root search around  $k = f/(2\pi c_T)$ .

The same root and mode selection technique is used as the one implemented for 2D SAFE, see Section 5.2.1.

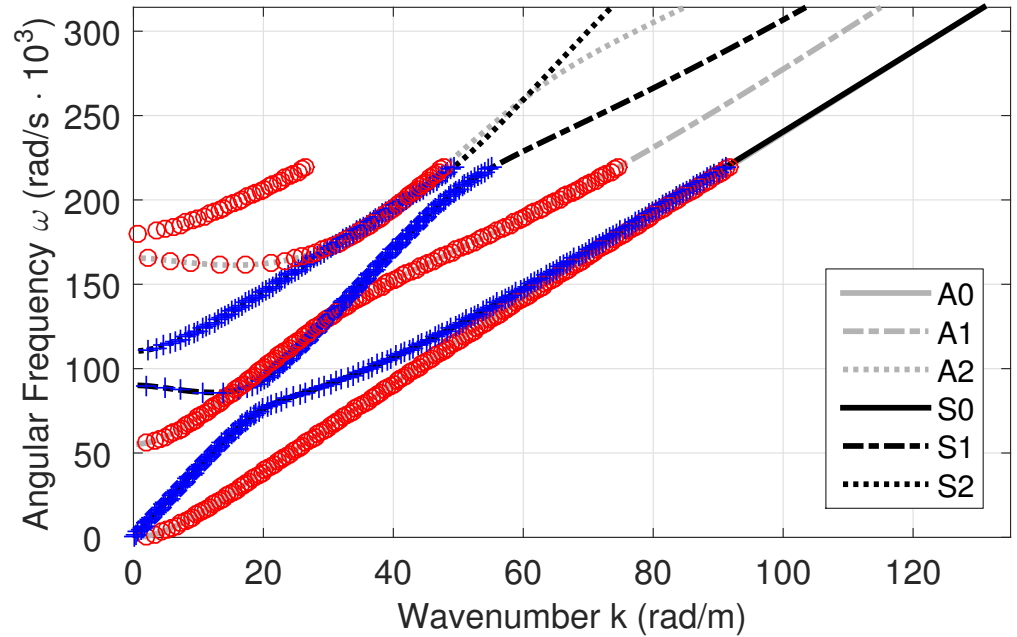
### 5.2.3 Results

The SAFE method captures accurately the dispersion relations. In Figure 5.3a the phase velocity of real valued roots from the SAFE method are plotted against DISPERSE dispersion curves for the six lowest modes, i.e. those shown in Figure 3.3a. SAFE phase velocity solutions are found along the dispersion curves. In Figure 5.3b the wave number of real valued roots from the SAFE method are plotted against DISPERSE wave number for the six lowest modes, i.e. those shown in Figure 3.3b. Roots that do not fit DISPERSE reference curves represent higher anti-symmetrical mode  $A_4$ . The roots of 1D SAFE and 2D SAFE coincide. Thus, the computational gains by using a 1D SAFE makes it the preferred method for symmetrical cross-sections.

Furthermore, the SAFE method manages to capture the SH waves, for both 1D and 2D SAFE, since no reduction of the wave field is made in (4.8). The roots of the SH modes are shown in Figure 5.4. A total of four SH modes,  $(SH_0, \dots, SH_3)$ , are found.



(a)



(b)

Figure 5.3: SAFE solution for symmetric (+), anti-symmetric (o) modes plotted against DISPERSE reference curves for the six lowest Lamb modes for a homogeneous isotropic linear elastic free plate.

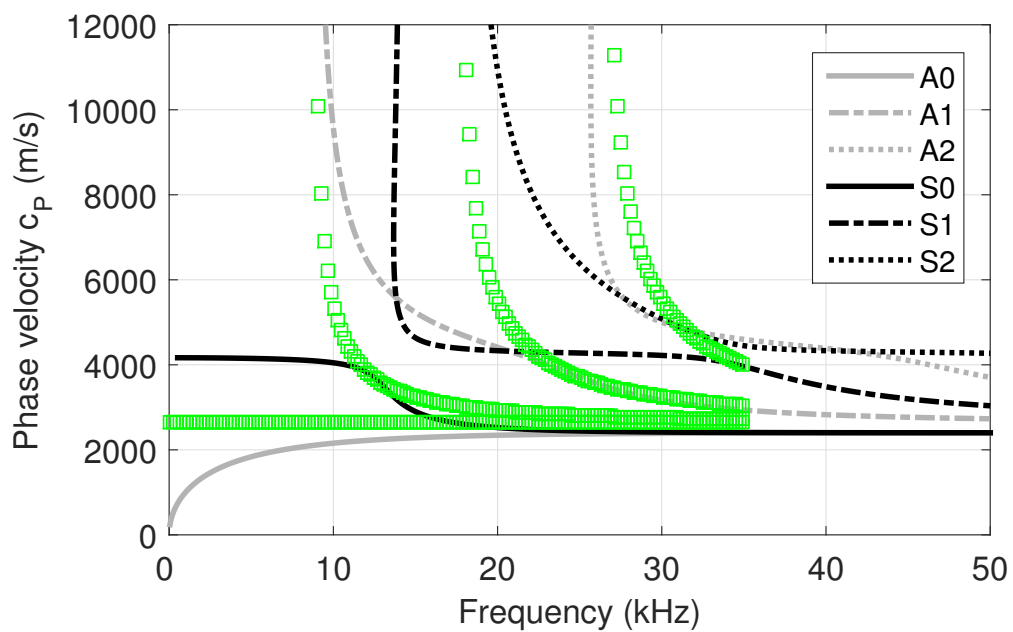


Figure 5.4: Energy velocity SAFE solution for horizontally polarized shear modes, SH modes, ( $\square$ ) plotted against DISPERSE reference curves for the six lowest Lamb modes for a homogeneous isotropic linear elastic free plate.

## 5.3 Extended properties for guided wave propagation

In this section we'll look into some extended properties of the wave propagation, that may be assessed by the set of wave number solutions and its corresponding eigenvectors,

1. group and energy velocity,
2. lossless excitability.

### 5.3.1 Group and energy velocity

The velocity of a wave group is called its group velocity,

$$c_{gr} = \frac{\partial \omega}{\partial k} .$$

In other words the velocity whereby the overall shape of the wave propagates. However, the concept of group velocity is not defined for damped wave guides. Instead, one need to consider the wave energy velocity,

$$c_E = \frac{\int_{\Omega} \langle P_{x_3} \rangle_t d\Omega}{\int_{\Omega} \langle E_{tot} \rangle_t d\Omega}$$

where  $\langle P_{x_3} \rangle_t$  is the time-averaged Poynting vector in the wave propagation direction. In other words, the time-averaged acoustic power flow along the wave guide, given by

$$\begin{aligned} \langle P_{x_3} \rangle_t &= -\frac{1}{2} \operatorname{Re} (\dot{u}_j^* \sigma_{3j}) \\ &= -\operatorname{Re} \left( \frac{i\omega}{2} u_j^* \sigma_{3j} \right) , \end{aligned}$$

and  $\langle E_{tot} \rangle_t$  is the time-averaged total energy, given by the sum of time-averaged kinetic energy,

$$\langle E_T \rangle_t = \frac{1}{4} \dot{u}_i^* \rho \dot{u}_i = \frac{\omega^2}{4} u_i^* \rho u_i ,$$

and time-averaged strain energy,

$$\langle E_W \rangle_t = \frac{1}{4} \sigma_{ij} \epsilon_{ij}^* = \frac{1}{4} \epsilon_{kl} C_{ijkl} \epsilon_{ij}^* ,$$

(Bartoli et al., 2006). For an undamped medium the energy velocity is equal to the group velocity (Auld, 1973).

### 5.3.2 Lossless Excitability

Excitability is defined as the ratio between the amplitude of the displacement response and the excitation force, for a given mode. In other words, it is the modal displacement frequency response to an applied force associated with that mode. The contribution of each mode may be summed to create the excited field. Hence, it may be determined which mode that will be dominant for a given excitation. Thereby, the NDT inspection system setup may be optimized in terms of sensor type and location ([Treysse and Laguerre, 2013](#)).

Let's consider a lossless wave guide (i.e. an undamped wave guide). Let the *lossless excitability* for a given mode  $m$  be,

$$e_{ij}^{(m)} = \frac{i\omega}{4 \int_{\Omega} \langle P \rangle_t d\Omega} U_i^{(m)} U_j^{(m)*},$$

where  $U_i^{(m)} = \{U_1^{(m)}, U_2^{(m)}, U_3^{(m)}\}$ . The structural response to an excitation is, thus, given by the sum of modal contributions,

$$U_i = \sum_{m=1}^M e_{ij}^{(m)} F_j^{(m)} e^{i k_m x_3},$$

where  $i = \sqrt{-1}$ ,  $F_j^{(m)}$  is the distribution of applied forces associated with mode  $m$  and  $M$  is the number of propagating modes. Lossless excitability is, thus, restricted to propagating modes in lossless wave guides. In other words, a system where the coefficient matrices are real valued and, hence, have real valued wave number roots corresponding to propagating modes. Furthermore, since non-propagating modes are excluded, lossless excitability is only valid in the far-field, where the contribution of evanescent waves to the excited displacement field are small ([Treysse and Laguerre, 2013](#)).

### 5.3.3 1D SAFE Implementation

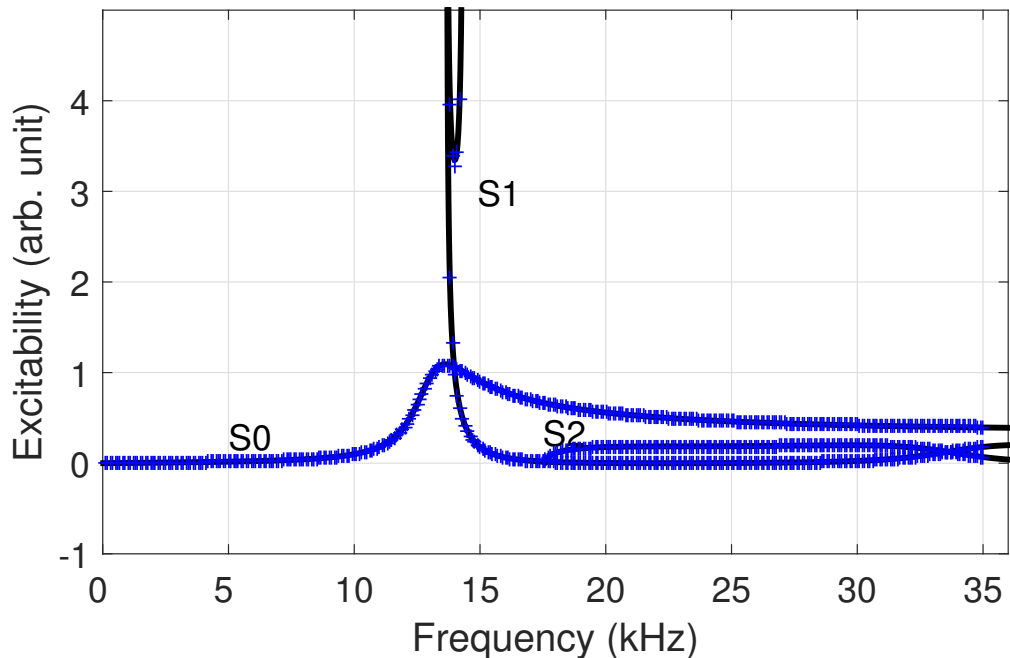
A 1D SAFE model is used to solve the dispersion relations. The domain is partitioned into 106 quadratic line elements. The dispersion relations are solved for 350 frequencies between 100 Hz and 35 kHz. The eigenvalue search is truncated at 80 wave number roots, with a centre of root search around  $k = f/(2\pi c_T)$ .

No damping is introduced into the system. Hence, propagating modes are represented by real valued wave number roots.

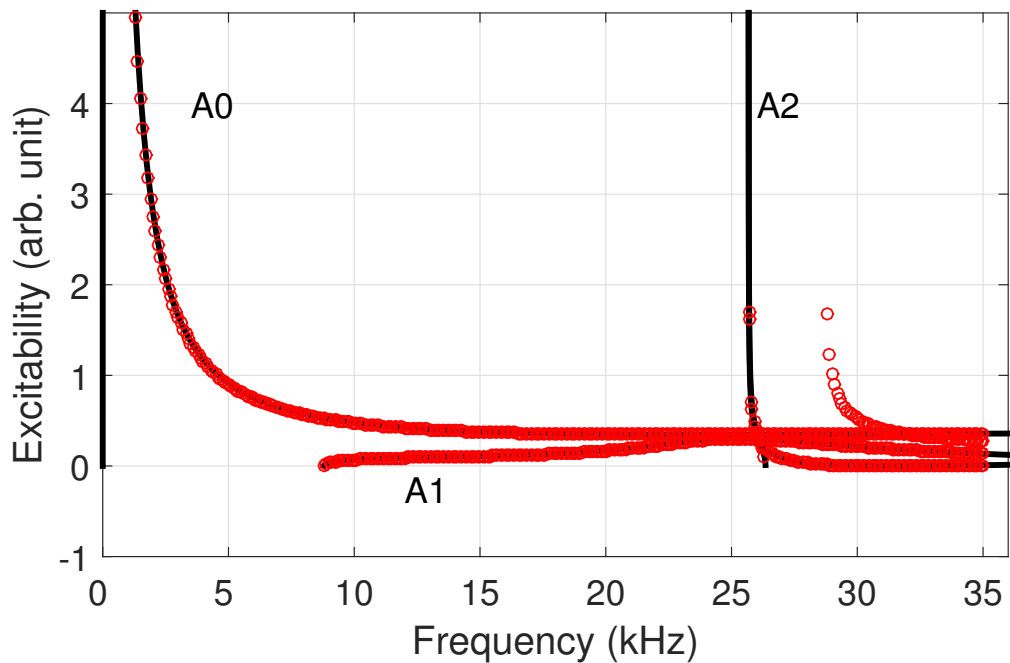
### 5.3.4 Results

In Figure 5.5 the lossless excitability for an applied force normal to the plate at the upper boundary, where the displacement is measured in the same point, is shown. The SAFE solutions accurately predicts the lossless excitability of the plate. In Figure 5.5b some SAFE roots do not fit the DISPERSE reference curves. These roots represent higher anti-symmetrical mode  $A_4$ , also visible in Figure 5.3.

Furthermore, the SAFE solutions successfully predicts the energy velocity of the plate, see Figure 5.6. The SAFE roots of higher anti-symmetrical mode  $A_4$  are visible, starting at 28 kHz.



(a)



(b)

Figure 5.5: Lossless excitability SAFE solution for (a) symmetric (+) and (b) anti-symmetric (○) modes plotted against `DISPERSE` reference curves for the six lowest Lamb modes for a homogeneous isotropic linear elastic free plate.

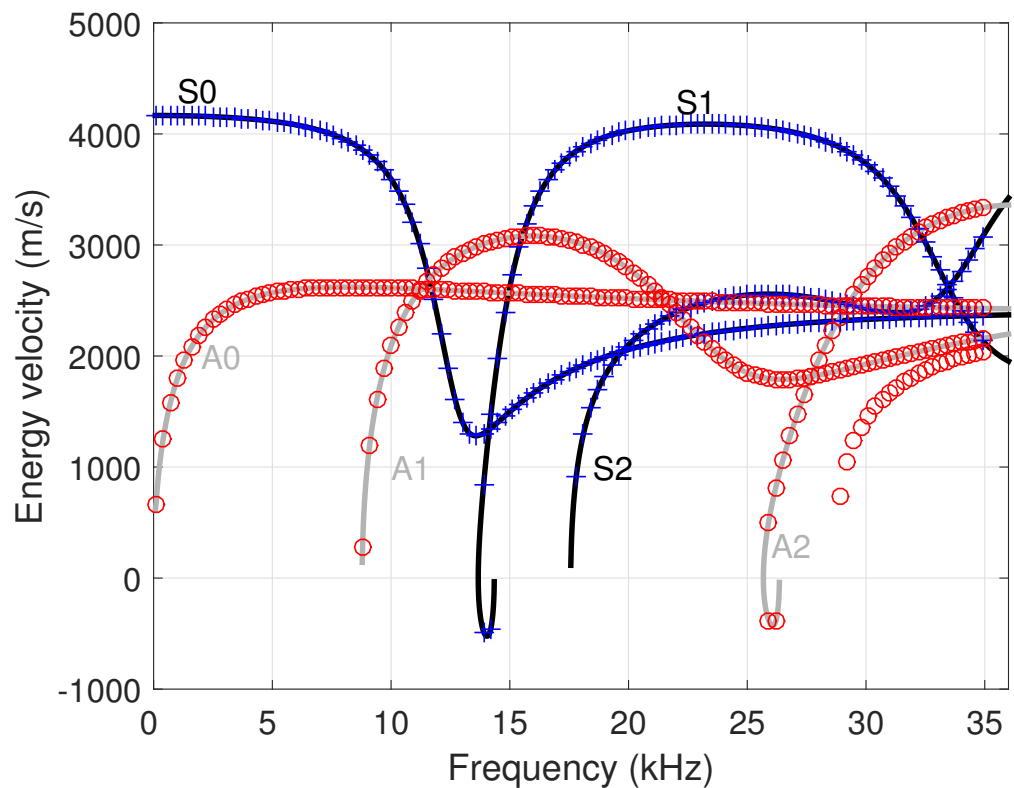


Figure 5.6: Energy velocity SAFE solution for symmetric (+), anti-symmetric (○) modes plotted against DISPERSE reference curves for the six lowest Lamb modes for a homogeneous isotropic linear elastic free plate.

## 5.4 Effects of damping

In the context of NDT application it is of interest to consider the attenuation. Let the attenuation be the reduction of the signal amplitude with respect to propagation distance. Hence, the amount of a body that may be inspected, from a given location, is dependent on the attenuation of the particular mode chosen. Attenuation of the lamb wave depends on several phenomena:

1. signal spreading due to dispersion,
2. signal spreading due to beam divergence (i.e. geometrical spreading),
3. material damping,
4. scattering,
5. leakage into surrounding media,

(Wilcox et al., 2001). In this section we'll consider the third phenomena more in-depth. Let's consider the effects of damping by introducing proportional damping for the plate in Section 5.2. A hysteretic model where the damping is proportional to the elasticity is used. Consequently, the complex elasticity tensor (2.7) is,

$$C_{ijkl} = C'_{ijkl} + i c_1 C'_{ijkl},$$

where  $c_1$  is a constant.

### 5.4.1 1D SAFE Implementation

Let's consider the plate in Table 5.1 of Section 5.2. A 1D SAFE model is used to solve the dispersion relations. A parametric study of the damping, for  $c_1 = \{1 2 4 8 10\} \%$  is made. The domain is partitioned into 106 quadratic line elements. The dispersion relations are solved for 333 frequencies between 100 Hz and 50 kHz. The eigenvalue search is truncated at 100 wave number roots, with a centre of root search around  $k = f/(2\pi c_T)$ .

Wave number roots where the ratio,

$$\frac{\text{Im } k}{\text{Re } k} \leq 4 c_1 ,$$

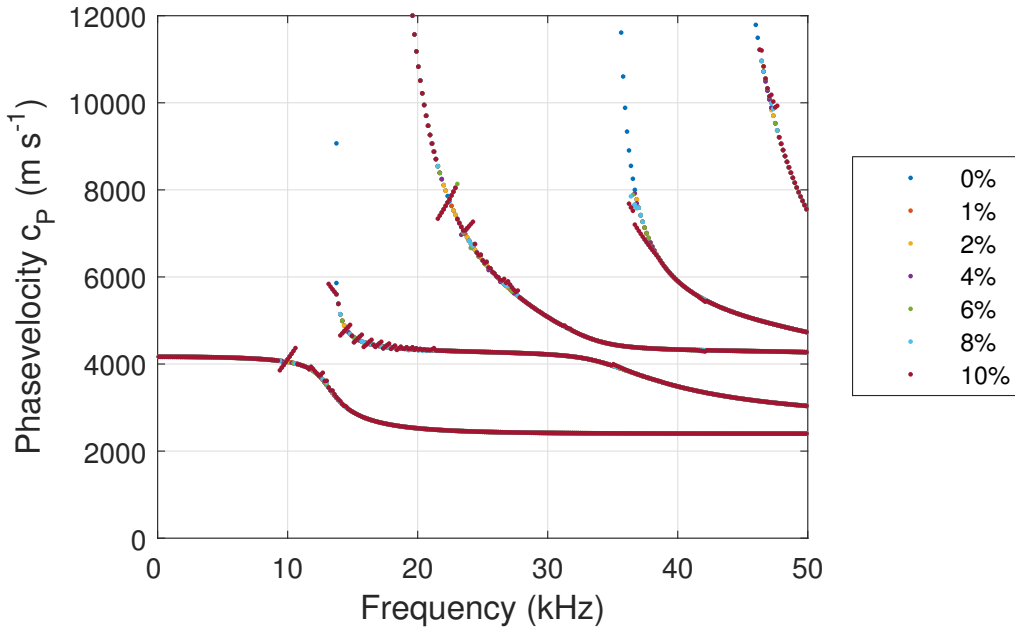
is satisfied are considered propagating modes.

### 5.4.2 Results

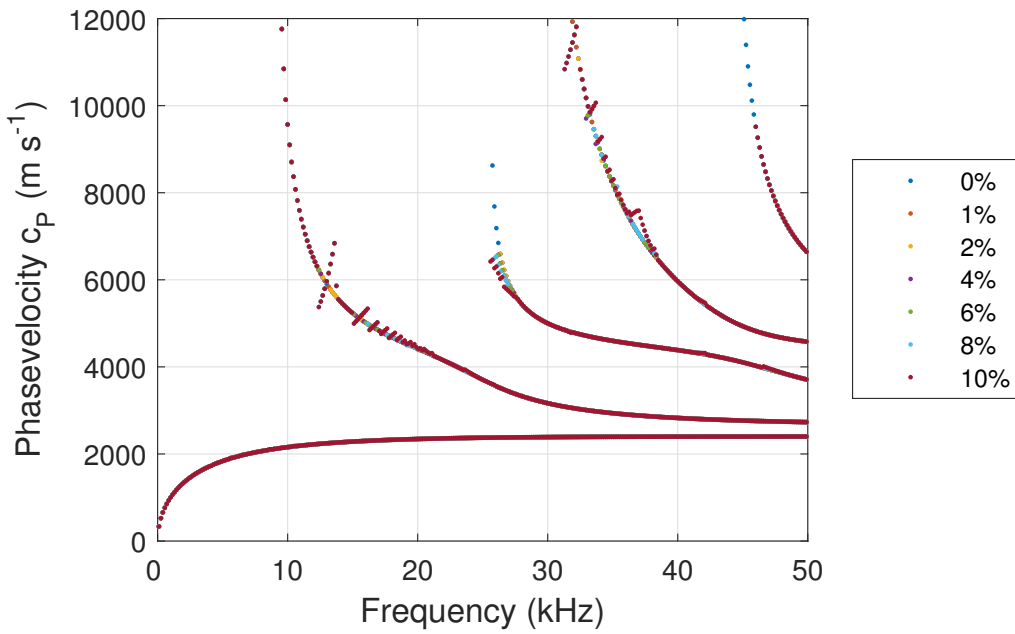
The change of the phase velocity, see Figure 5.7, and the real part of the wave number, see Figure 5.8, is small with increasing damping. A deviation from the undamped curves occurs close to the cut-off frequencies. There occurs a plume of roots, visible as bands of roots perpendicular to the general trend. These plumes are assumed to be numerical noise.

Similarly, lossless excitability, see Figure 5.9, is not significantly affected by increased damping.

In conclusion, it may be stated that introducing proportional hysteretic damping, where the damping does not exceed 10 % of the stiffness, to a continuous homogeneous isotropic linear elastic free plate, have a small, and presumably negligible, effect on the solution to the phase velocity and lossless excitability. Hence, for practical inspection applications an undamped model may, presumably, be sufficient as a conceptual model for a lightly damped plate. However, increasing damping implies increasing levels of attenuation, which affects the feasible range of inspection, from a given point on the structure.



(a)



(b)

Figure 5.7: Phase velocity SAFE solution for (a) symmetric and (b) anti-symmetric modes for a lightly damped plate.

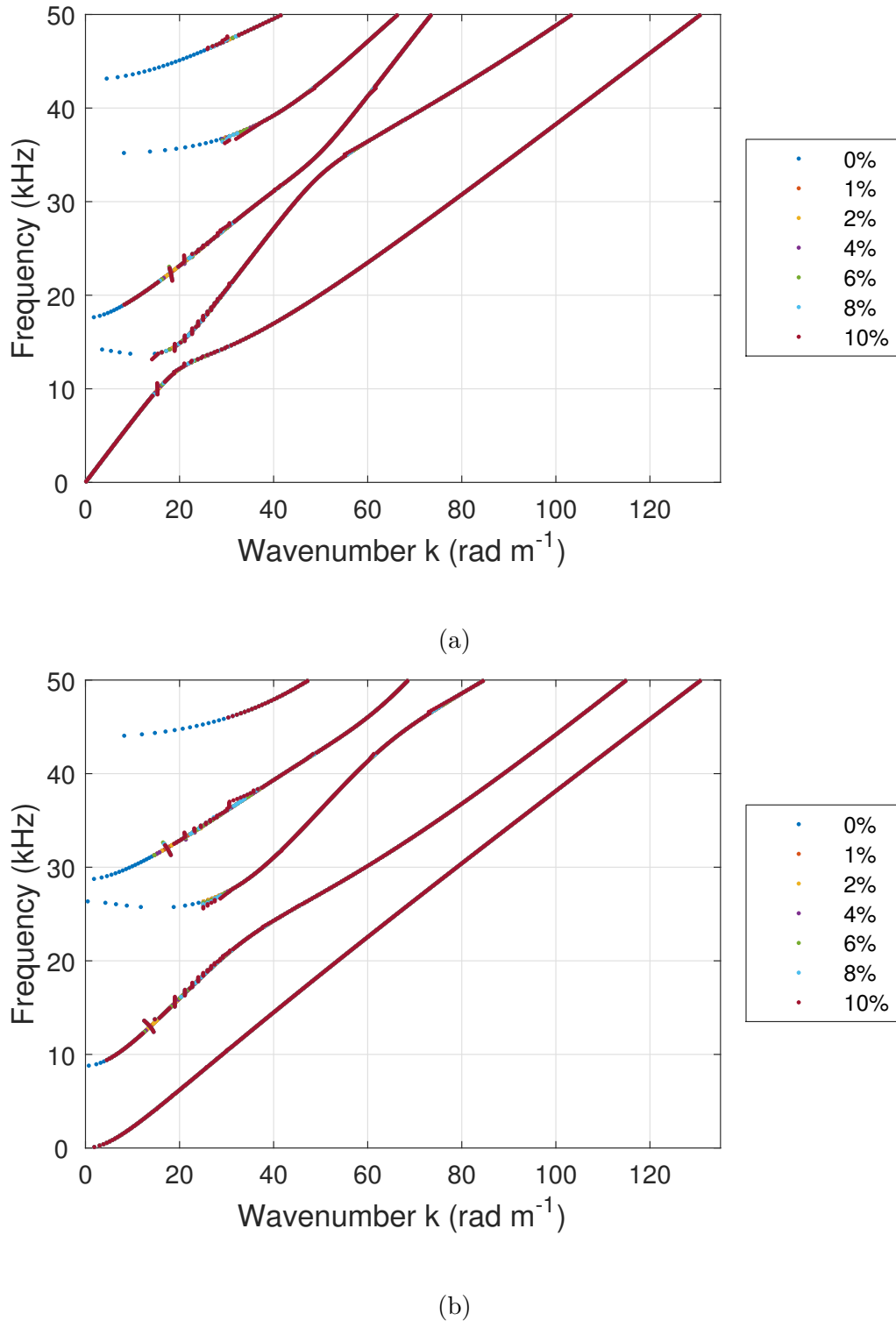
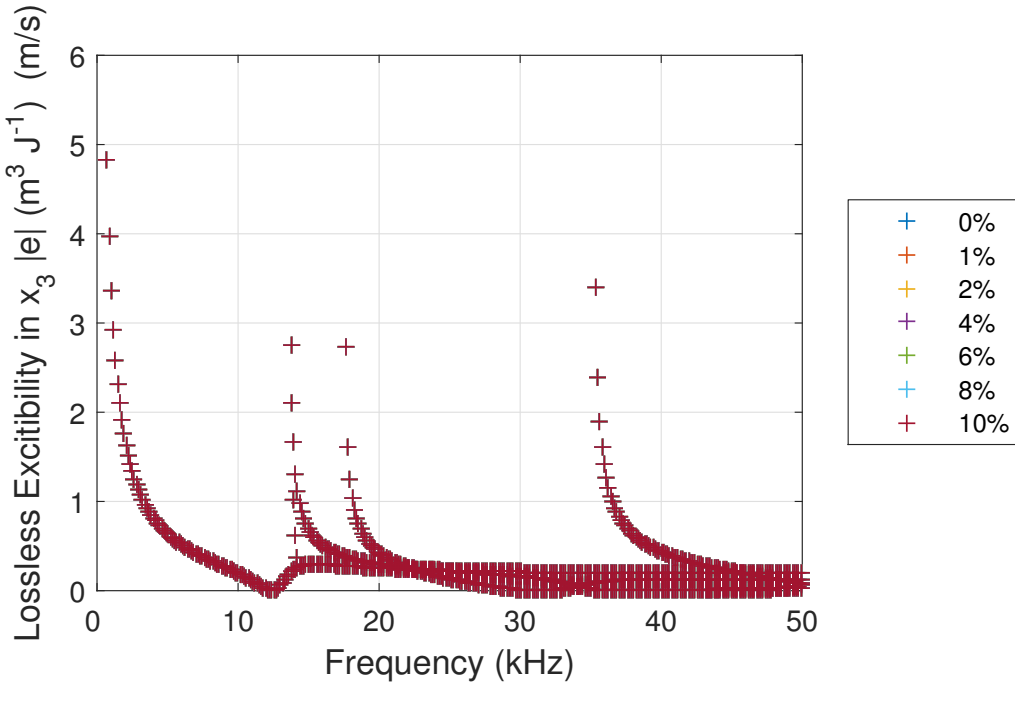
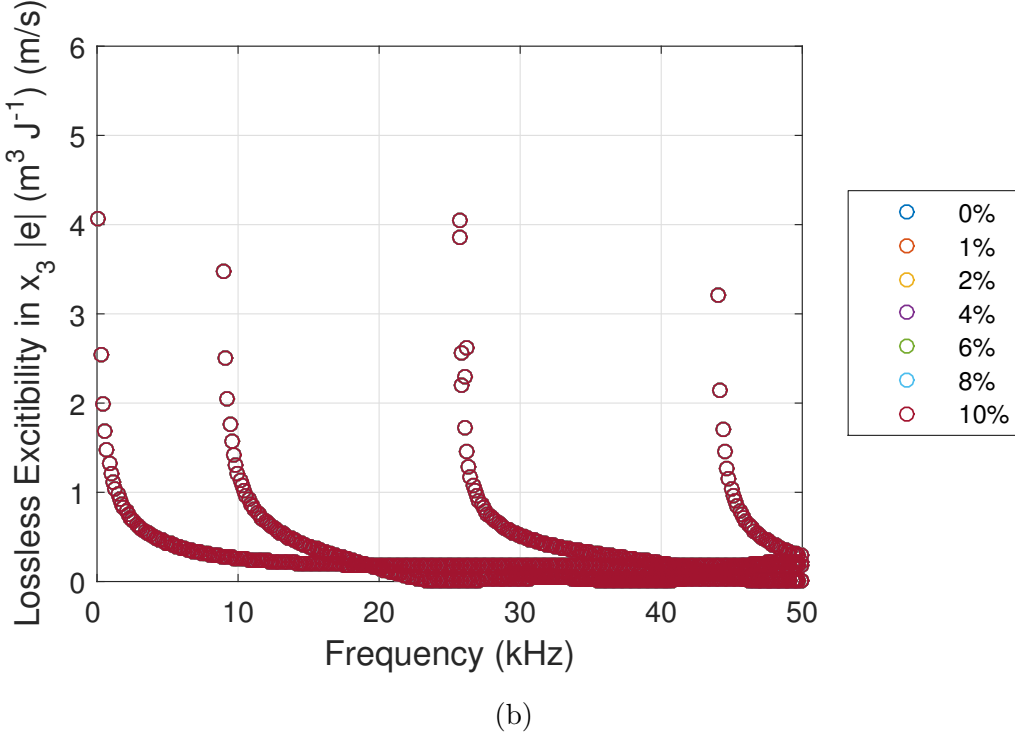


Figure 5.8: Wave number SAFE solution for (a) symmetric and (b) anti-symmetric modes for a lightly damped plate.



(a)



(b)

Figure 5.9: Lossless excitability SAFE solution for (a) symmetric (+) and (b) anti-symmetric (o) modes for a lightly damped plate.

## 5.5 Effects of stiffness gradient

In this section we'll consider the effects of introducing a stiffness gradient across the plate thickness. This is of particular interest when studying concrete plates. It has been measured (Popovics et al., 2006; Boyd and Ferraro, 2005) that the P-wave velocities are greater at the lower boundary than the upper boundary, due to aggregate settlement in the young concrete (Popovics et al., 2006) or sulphate attacks (Boyd and Ferraro, 2005).

For an isotropic homogeneous medium the P-wave velocity,

$$c_L = \sqrt{\frac{\lambda + 2\mu}{\rho}} = \sqrt{\frac{E}{\rho} \frac{(1 - \nu)}{(1 + \nu)(1 - 2\nu)}}$$

is a function in the square root of Young's modulus  $E$ .

The P-wave velocity is of particular interest because of its use in estimating plate thickness using modes with zero group velocity (Baggens and Ryden, 2015). When the group velocity is zero the wave group propagation velocity is zero but the phase velocity remains non-zero. Thus, it exists localized resonance. In the frequency range of interest, 100 Hz to 35 kHz, there exists two zero group velocity (ZGV) modes: an  $S_1$  mode at circa 13 kHz and an  $A_2$  mode at circa 26 kHz, see Figure 5.6. The frequency of the first detectable ZGV mode may be estimated by the empirical formula,

$$f_r = \beta \frac{c_L}{2h}, \quad (5.1)$$

where  $\beta$  is a correction factor ( $\simeq 0.96$  for concrete) and  $h$  the plate thickness. The frequency  $f_r$  correspond to the  $S_1$  ZGV frequency (Baggens and Ryden, 2015). Consequently, by measuring the P-wave velocity and  $S_1$  ZGV frequency one may estimate the thickness. However, in concrete plates one may be restricted to one sided access to the plate (e.g. foundations). Hence, if there exists a gradient in the P-wave velocity over the thickness, the measured P-wave velocity at the surface may yield an incorrect thickness estimate.

### 5.5.1 1D SAFE Implementation

Let's consider the plate in Table 5.1 of Section 5.2. A P-wave velocity gradient is introduced by using a linear distribution of Young's Modulus  $E$  from  $(1-\alpha)E_0$  on the upper boundary to  $(1+\alpha)E_0$  at the lower boundary, where  $E_0$  is equal to 40 GPa, see Table 5.1, and the gradient coefficient  $\alpha$  is equal to 10

%. A 1D SAFE model is used to solve the dispersion relations. The domain is partitioned into 106 quadratic line elements. The dispersion relations are solved for 236 frequencies between 13 570 Hz and 14 040 Hz, the frequency range of interest for the S<sub>1</sub> ZGV mode. The eigenvalue search is truncated at 100 wave number roots, with a centre of root search around  $k = f/(2\pi c_T)$ .

No damping is introduced into the system. Hence, propagating modes are represented by real valued wave number roots.

### 5.5.2 Results

The effects of a gradient on the phase velocity is shown in Figure 5.10a, and on the wave number roots in Figure 5.10b. The S<sub>1</sub> ZGV frequency have shifted some. From a frequency of circa 13 672 Hz for the gradient-less plate to circa 13 666 for a plate with a ± 10 %-gradient. The phase velocity at the ZGV frequency is slightly greater for the ± 10 %-gradient plate and, thus, the corresponding wave number is slightly lower than for the gradient-less plate. It may be concluded that the ratio between ± 10 %-gradient ZGV frequency and gradient-less ZGV frequency,

$$\frac{f_r|_{\alpha=10\%}}{f_r|_{\alpha=0}} \approx 1 .$$

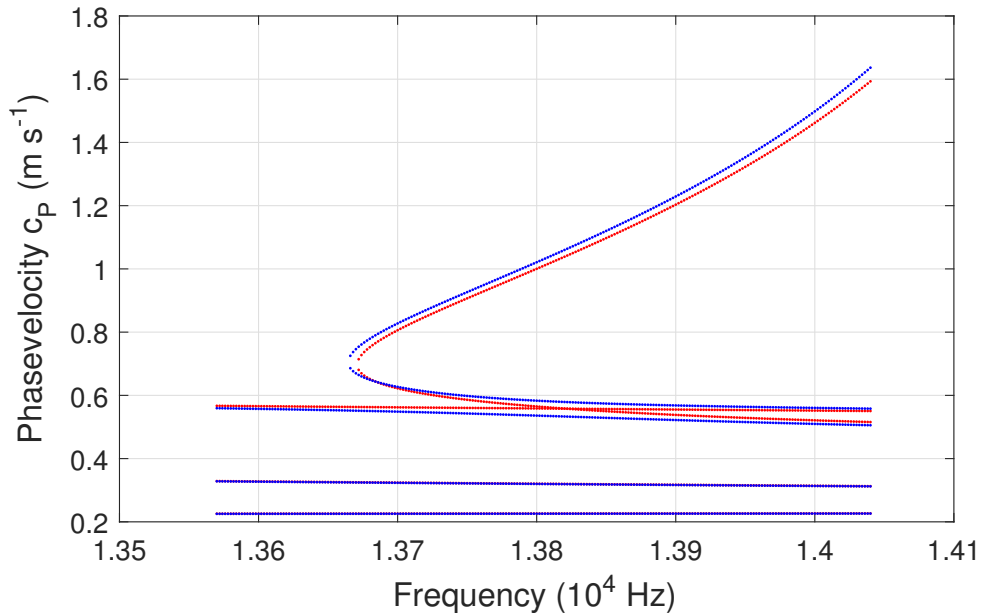
Hence, error due to ZGV frequency shift is negligible compared to that which arises due to an incorrect longitudinal velocity  $c_L$ . The error in thickness estimate is, roughly, proportional to the error in the P-wave velocity estimation,

$$\frac{h|_{\alpha=10\%}}{h|_{\alpha=0}} \propto e(c_L) .$$

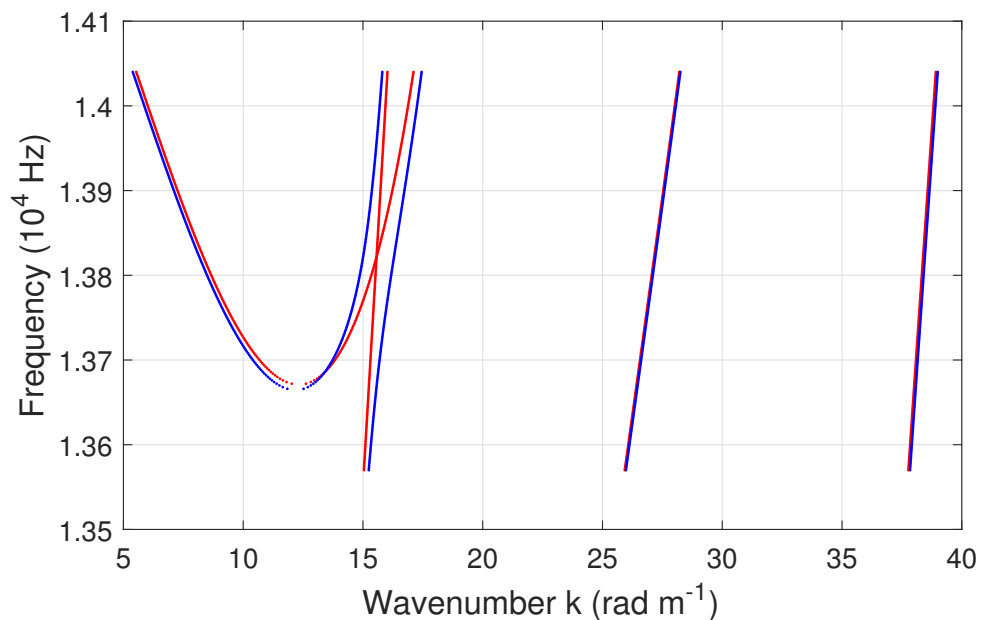
If one assumes that access is only allowed on the upper boundary for measurements of the P-wave velocity, and that only the upper boundary P-wave velocity is measured, then  $e(c_L) = (1 - \Delta\alpha) = 90\%$ .

At the ZGV frequency no roots are displayed. This is due to that the wave number roots no longer are real valued. In other words the wave number root is complex valued and, thus, represent an evanescent mode. The group velocity (i.e. same as energy velocity for undamped plates) is shown in Figure 5.11a. The lossless excitability is shown in Figure 5.11b. Around the ZGV frequency the excitability increases rapidly. Hence, the ZGV is easier to excite compared to other modes and, thus, is more detectable compared to other modes, at the same frequency. As previously stated, lossless excitability may only capture the excitability of propagating modes. Consequently,

the excitability is not given at the ZGV frequency where the mode becomes evanescent.

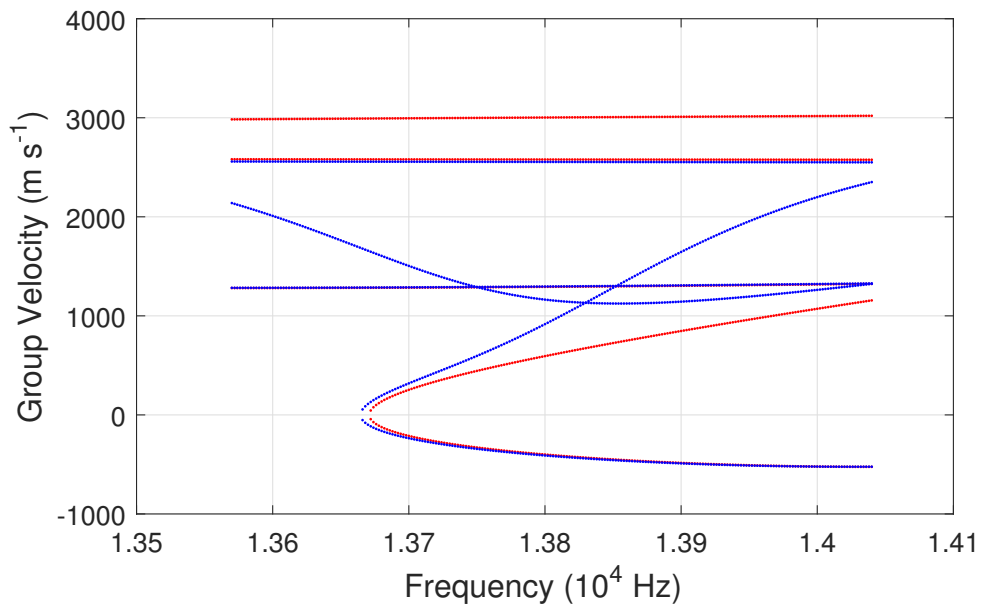


(a)

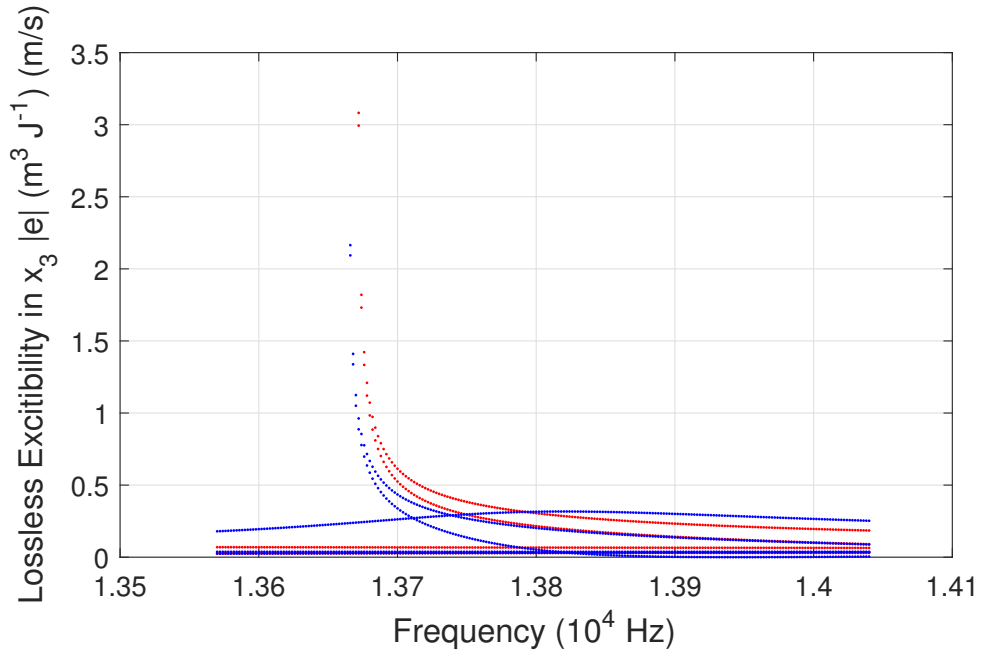


(b)

Figure 5.10: SAFE solution for no gradient (—) modes plotted against  $\pm 10\%$  gradient (—) modes.



(a) Group Velocity



(b) Lossless Excitability

Figure 5.11: Lossless excitability SAFE solution for no gradient (—) modes plotted against  $\pm 10\%$  gradient (—) modes.

## 5.6 Leaky characteristics and unbounded domains

In the preceding cases it's presumed that the boundaries are stress free. However, an important class of problems occur when the wave propagating along the wave guide radiate into a unbounded surrounding media. This is referred to as the structures *leaky* characteristic, since energy radiates ("leaks") from the wave guide into the unbounded medium. In this section we'll consider a multi-layered half-space; namely, a pavement structure.

The pavement structure may be modelled using a three layer model, as proposed by [Ryden and Lowe \(2004\)](#). The layer parameters are given by Table 5.2, where Layer 3 is an unbounded half-space, i.e. infinite in its extent. The upper boundary is assumed stress free. To model the infinite

Table 5.2: Characteristics of a three-layer pavement structure.

|                     | $c_T$ (m/s) | $c_L$ (m/s) | $\rho$ (kg/m <sup>3</sup> ) | Damping | Thickness (m) |
|---------------------|-------------|-------------|-----------------------------|---------|---------------|
| Layer 1 (Asphalt)   | 1400        | 2914        | 2000                        | None    | 0.2           |
| Layer 2 (Grade)     | 500         | 1041        | 2000                        | None    | 0.6           |
| Layer 3 (Sub-grade) | 100         | 208         | 2000                        | None    | $\infty$      |

domain of a half-space within the finite domain of a FE-model some numerical approximation of the half-space is necessary. The requirement on such an approximation is that any wave entering the half-space should continue its propagation, and not be reflected back into the computational domain. This may be achieved through several approaches, such as *non-reflecting boundary conditions* (NRBC), *perfectly matching layers* or *absorbing regions* (AR) ([Drozdz et al., 2006](#)). We'll consider an approximation using absorbing regions, as it has a robust performance for general use ([Fan et al., 2013](#)). In an AR approach a non-physical domain with large attenuation is added to the computational domain. Hence, incident waves are absorbed within the absorbing region. To avoid large impedance differences, and thus spurious reflections, a damping factor  $D(r)$  is introduced,

$$D(r) = \begin{cases} \alpha_A \left( \frac{r - r_A}{L_A} \right)^n & \text{if } r \geq r_A \\ 0 & \text{otherwise} \end{cases}$$

where  $L_A$  is the length of the absorbing region,  $r$  is the position,  $r_A$  is the starting position of the absorbing region,  $n$  is the degree and  $\alpha_A$  is a scaling

parameter. Hence the complex elasticity tensor is,

$$C_{ijkl} = C'_{ijkl} \left(1 - D(r)\right) + i \left(C''_{ijkl} + C'_{ijkl} D(r)\right) \quad (5.2)$$

within the absorbing region (Ke et al., 2009). The real part of the elasticity tensor is decreasing and the imaginary part is increasing with increasing distance from the computational domain. Consequently, the stiffness is decreasing and damping is increasing with increasing distance. To minimize impedance mismatch further, a complex valued density  $\rho$  is introduced,

$$\rho = \frac{1}{1 - D(r) + iD(r)} \rho_0. \quad (5.3)$$

The distribution of  $\rho$  for different  $\alpha_A$  values is shown in Figure 5.13 and for different degrees  $n$  in Figure 5.12. The parameters  $\alpha_A$  and  $n$  are chosen as 1 and 3, respectively. In other words, the damping factor is a monotonically increasing cubic function in the distance with in the absorbing region, scaled with a factor 1.

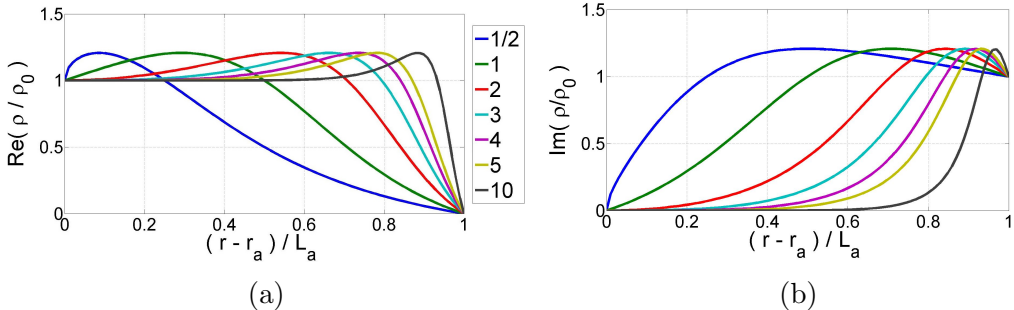


Figure 5.12: (a) Real part of  $\rho$  for different  $n$ , (b) imaginary part of  $\rho$  for different exponents  $n$  to the loss factor, within the absorbing region,  $\alpha_A = 1$ .

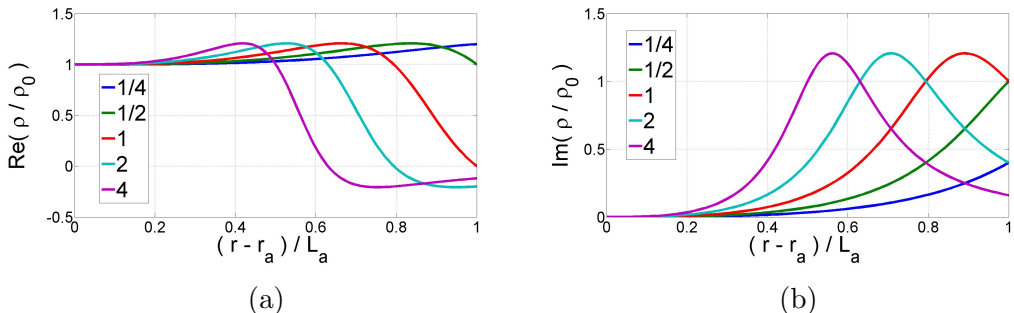


Figure 5.13: (a) Real part of  $\rho$  for different  $\alpha$ , (b) imaginary part of  $\rho$  for different  $\alpha$  within the absorbing region,  $n = 3$ .

A heuristic approach for defining the radiated wavelength is proposed by [Castaings and Lowe \(2008\)](#). A rough estimate of the smallest phase velocity of all modes  $M$ ,  $\min(c_M)$ , in the relevant frequency range can be obtained by solving for the free plate. Using Snell's Law the maximum radiation angle,

$$\max(\theta_{rad}) = \arcsin\left(\frac{c_{L,rad}}{\min(c_M)}\right),$$

is obtained, whereby the projection of the radiated wavelength onto the cross-section  $x_2$ -direction,

$$\max(\lambda_{x_2}) = \frac{\max(\lambda_{rad})}{\cos[\max(\theta_{rad})]}$$

yields the number of cycles of the radiated wave in the most unfavourable situation ([Castaings and Lowe, 2008](#)). To assure that no waves are reflected back into the computational domain, the size of the absorbing region is set to a minimum of 1.5 times the projected wavelength of the radiated wave with maximum radiation angle ([Ke et al., 2009](#)). In Figure 5.14 its shown (a) a too small absorbing region and (b) a sufficiently large absorbing region.

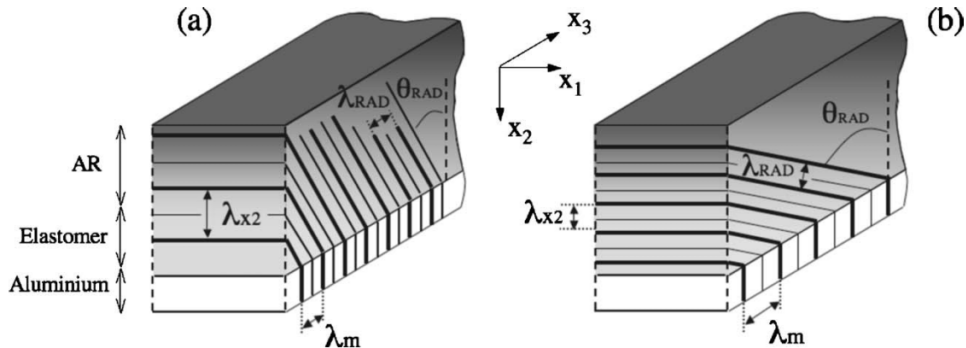


Figure 5.14: (a) Ill-defined absorbing region and (b) well-defined absorbing region. Picture taken from [Castaings and Lowe \(2008\)](#)

### 5.6.1 1D SAFE Implementation

A 1D SAFE model is used to solve the dispersion relations. The domain is partitioned into 400 quadratic line elements. The dispersion relations are

solved for 191 frequencies between 100 Hz and 2 kHz. The eigenvalue search is truncated at 100 wave number roots, with a centre of root search around  $k = f/(2\pi \min [c_T])$ . The absorbing region is set to 4 meters or 2.5 times the projected wavelength of the radiated wave with maximum radiation angle in frequency range of interest.

Wave number roots where the ratio,

$$\frac{\operatorname{Im} k}{\operatorname{Re} k} \leq \beta_k ,$$

is satisfied are considered propagating modes. To remove spurious wave number roots, that exist due to resonance in the non-physical domain, a power flow criteria is used. If the space and time averaged power flow integrated over the computational domain ( $\Omega_{CD}$ ) is greater than the space and time averaged power flow integrated over the absorbing region ( $\Omega_{AR}$ ) multiplied by some selection factor  $\beta_P$ ,

$$\frac{1}{\Omega_{CD}} \int_{\Omega_{CD}} \langle P_{x_3} \rangle_t d\Omega \geq \beta_P \frac{1}{\Omega_{AR}} \int_{\Omega_{AR}} \langle P_{x_3} \rangle_t d\Omega ,$$

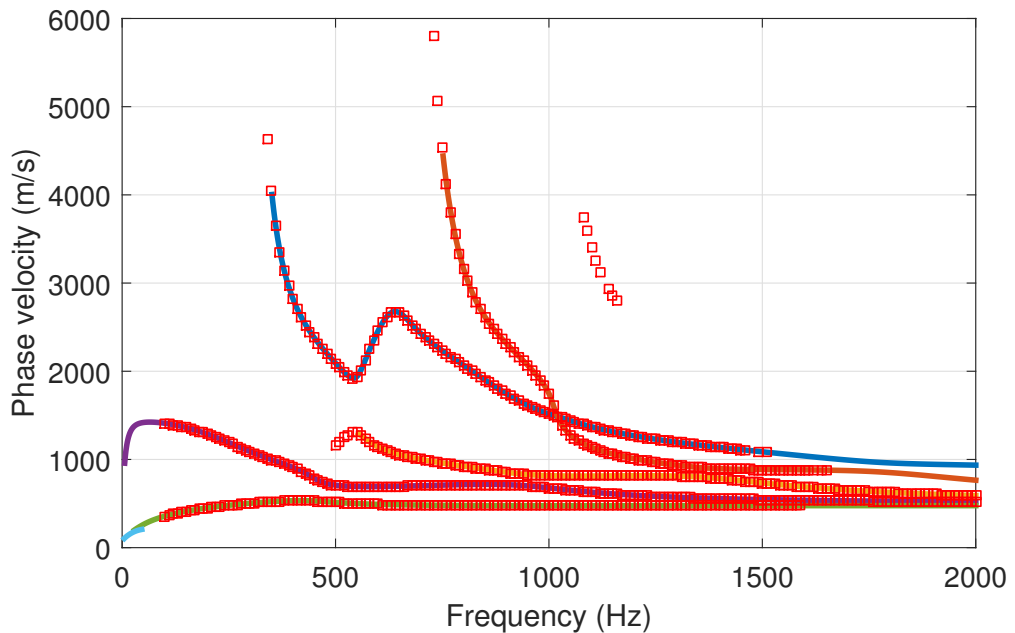
then the mode is selected.

### 5.6.2 Results

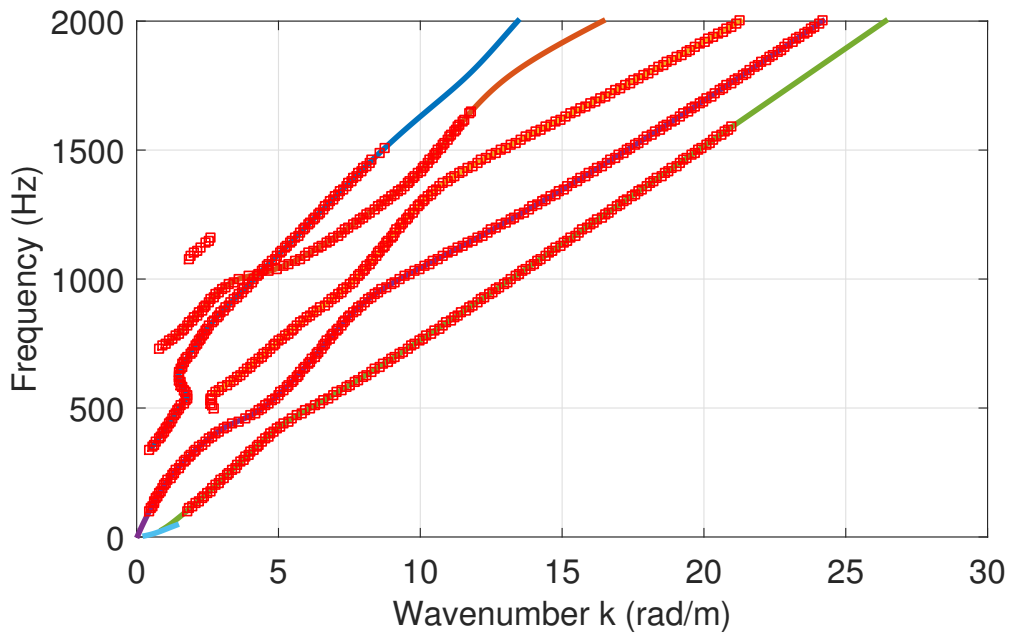
Modes are chosen by setting  $\beta_P$  equal to 1 and  $\beta_k$  equal to 0.55 (55%). The phase velocity, see Figure 5.15a, may be captured correctly by simulating an unbounded half-space with an absorbing region. Similarly, the wave number roots, see Figure 5.15b, are aligned. Furthermore, the group of SAFE solutions that do not fit a DISPERSE reference curve represent a higher mode, that was not solved for, using DISPERSE.

In using an absorbing region, complex valued coefficient matrices are introduced. Hence, lossless excitability is, strictly speaking, not applicable. However, the general characteristics of the plates excitability may be captured using lossless excitability, see Figure 5.16. The lossless excitability is normalized with respect to the power flow integrated over the computational domain (□), and with respect to the power flow integrated over all domains (□) (both computational domain and absorbing region), respectively. The fit is considerably better if one normalizes with respect to the computational domain, rather than all domains. It would be of considerable interest in further studies to determine whether this is due to the fact that no damping is introduced into the computational domain, or to the large increase in

damping in the computational domain. The underlying question would be, at what limit does lossless excitability no longer capture a general shape and magnitude of the excitability curve.



(a)



(b)

Figure 5.15: SAFE solution for all ( $\square$ ) modes plotted against DISPERSE reference curves for the six lowest Lamb modes for a pavement structure.

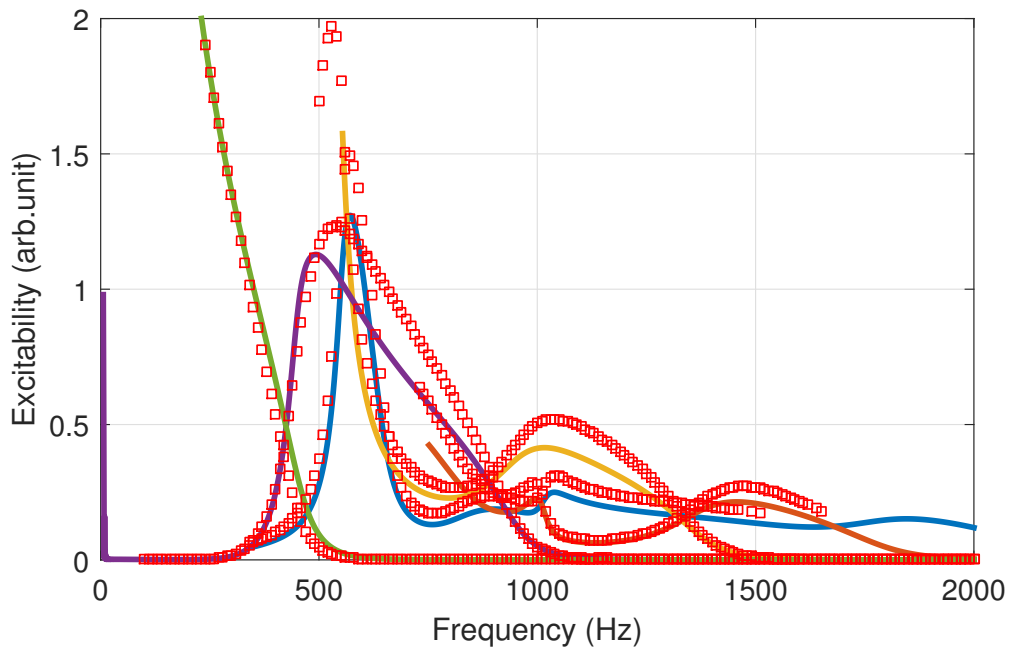
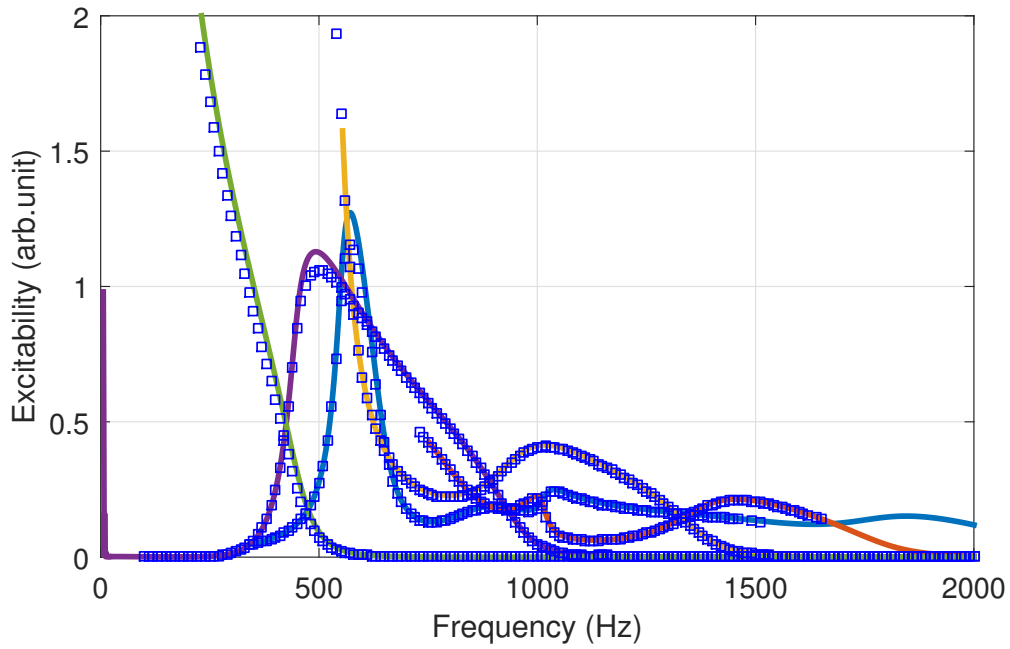


Figure 5.16: Lossless excitability normalized with respect to the computational domain ( $\square$ ), and normalized with respect to both computational domain and absorbing region ( $\square$ ), plotted against DISPERSE reference curves for the six lowest Lamb modes for a pavement structure.



# Summary

## 6.1 Discussion

In this master's thesis, the capabilities of the Semi-Analytical Finite Element method (SAFE), and its implementation, is studied for civil engineering plate-like structures. It is shown that a SAFE discretisation using the commercial finite element software **COMSOL** successfully predicts the dispersion relations for plates. The validation of SAFE solutions is made against solutions from the matrix method software **DISPERSE**.

Fundamentally, SAFE is an eigenvalue problem. By exploiting the underlying eigenvalues and eigenvectors, it is shown that extended properties, such as energy velocity and lossless excitability, may be captured accurately. Furthermore, it is shown that using a 1D SAFE discretisation yields the same result as a 2D discretisation. As a result, considerable computational savings can be made in using a 1D formulation over a 2D formulation for simple symmetric geometries.

One of the capabilities of SAFE, that the various matrix methods lacks, is the ability to model arbitrary cross-sections. In this thesis no example of a plate with non-symmetrical cross-section is presented. However, it should be evident to the reader that more complicated cross-sections can be analysed, based on the theory presented. This is shown by implementing and solving the dispersion relations for a half-space. Albeit the half-space is not a plate, its discretisation is. The infinite extent of the half-space is modelled as a finite region with large attenuation; an absorbing region. Within the absorbing region both elasticity tensor and density become complex valued, representing the medium's attenuation. It is shown that using a monotonically

increasing cubic function to model an increasing attenuation with distance, successfully predicts the dispersion relations for a half-space. Thereby, an important class of civil engineering problems may be addressed: those where acoustic energy is radiated into an unbounded media. A half-space model have potential for modelling guided wave propagation in a wide variety of civil engineering structures: such as foundations, embankments and dams. It should be obvious to the reader that the use of an absorbing region is not limited to modelling half-spaces. It allows itself to generalization from infinite extent in one direction to infinite extent in both of the cross-section directions. From a civil engineering perspective, as proposed by [Castaings and Lowe \(2008\)](#), this allows for the modelling of guided waves along a steel rebar inside concrete with, nominally, infinite extent.

The introduction of an absorbing region foreshadows another important capability of SAFE: the ease whereby complex material models may be introduced. From a modelling perspective the absorbing region is a representation of the half-space. However, from a finite element perspective it may simply be viewed as domain with a peculiar material model. Hence, it may be stated that adding a material discontinuity is unproblematic. Thereby, it is straight forward to model a pavement structure, using a three phase approximation: asphalt, grade and sub-grade, as proposed by [Ryden and Lowe \(2004\)](#). The structure is, thus, represented by a three layered half-space . It is shown that the dispersion relations for such a structure is accurately captured by a SAFE discretisation. It should be obvious to the reader that such material discontinuities are not limited to layered media, but may have arbitrary shape in the cross-section domain.

Drawing fully from the capability of modelling the wave propagation using arbitrary material models, a parametric study of the effects of damping is made. It is shown that introducing proportional hysteretic damping where the damping does not exceed 10 % of the stiffness, have a small , and presumably negligible, effect on phase velocity and lossless excitability. From the perspective of practical inspection systems this is an important feature. If the plate is lightly damped, a conceptual model based on an undamped plate is sufficient to equate a measured phase velocity to a given mode.

It has been observed in concrete plates that there exists a P-wave velocity gradient over the plate thickness; presumably due to aggregate settlement in the young concrete ([Popovics et al., 2006](#)) and sulphate attacks ([Boyd and Ferraro, 2005](#)). If one adopts an isotropic material model for the concrete the P-wave velocity is proportional to the square root of Young's modulus. It

is shown that a constant linear gradient in Young's modulus over the thickness causes a small but not significant lowering of the  $S_1$  zero group velocity (ZGV) frequency. The lossless excitability and phase velocity for the  $S_1$  ZGV mode remains, roughly, the same. Hence, if one utilises the  $S_1$  ZGV mode for plate thickness estimation, the error due to frequency shift is negligible compared to errors that arise from incorrect P-wave velocities.

Moreover, it is shown that lossless excitability may potentially capture some aspects of the excitability of damped wave guides, albeit not being strictly defined for such wave guides. Considering the introduction of attenuation by an absorbing region into a multi-layered half-space; it is shown that, preferably, the lossless excitability should be normalized with respect to the power flow in the computational domain (i.e. physical domain) rather than both computational domain and absorbing region (i.e. both physical and non-physical domain).

One of the main assumptions in SAFE modelling is that the geometric and material properties are the same along the wave propagation direction. Although SAFE yields a three dimensional (3D) displacement field, it does so under rather strong assumptions of material and geometric uniformity. In fact, it is shown that this is the manner in which a 3D discretisation may be reduced to a 2D or 1D discretisation. Hence, SAFE is not a *true* discretisation of the three dimensional body, except if uniformity is fulfilled for the actual body or specimen. Anyone pursuing a SAFE discretisation need to be keenly aware of this.

Indeed, any deviation from the SAFE predictions, is the means by which a feature or damage is identified during inspections. That is, if one wish to asses the uniformity along the wave guide, a deviation from the prediction, is a sign that uniformity may not be fulfilled. Hence, SAFE may be considered a method whereby the statement; *the wave guide is uniform*, may be corroborated or disproved. Note, that this is a statement about the applicability of SAFE as a numerical scheme and not about the applicability of guided waves as an inspection method.

## 6.2 Conclusions

The aim of this master thesis is to implement and study the capabilities of the Semi-Analytical Finite Element method for civil engineering plate-like structures.

First, an introduction to the field of acoustic guided waves in plates is presented. Second, the SAFE mathematical framework and the underlying theory of quadratic eigenvalue problem is presented. Third, the SAFE is applied to four civil engineering plate-like structures: (1) a continuous homogeneous isotropic linear elastic free plate, (2) a continuous homogeneous isotropic linear elastic free plate with proportional hysteretic damping, (3) a continuous isotropic linear elastic free plate with a stiffness gradient and (4) a multi-layered half-space.

In this master's thesis it is shows that:

- for a a continuous homogeneous isotropic linear elastic free plate, the SAFE solutions to the dispersion relations align with those of matrix method solutions, provided by the software **DISPERSE**,
- for a symmetric cross-section a 1D SAFE discretisation is preferable to a 2D SAFE discretisation, with respect to computational time,
- the modal lossless excitability and energy velocity may be computed from the corresponding modal eigenvectors,
- introducing proportional hysteretic damping, where the damping does not exceed 10 % of the stiffness, to a continuous homogeneous isotropic linear elastic free plate, have a small, and presumably negligible, effect on the solution to the dispersion relations and lossless excitability,
- a linear gradient in Young's modulus over the thickness, where the gradient does not exceed  $0.9 E_0$  at the upper boundary and  $1.1 E_0$  at the lower boundary, have a small effect on the  $S_1$  ZGV frequency. Thus, error in thickness estimates using the empirical formula,

$$f_r = \beta \frac{c_L}{2h} ,$$

will not be significant due to a shift in  $S_1$  ZGV frequency.

- an absorbing region, with a uniaxial cubic damping factor, may be used to solve the dispersion relations for a multi-layered half-space.

In conclusion it may be said that SAFE successfully captures the dispersion relations of wave guides, with respect to matrix method solutions. The motivation for using SAFE, rather than matrix methods, is the ease whereby complex cross-section geometries and material models may be introduced. Hence, SAFE have a strong potential as a tool in creating conceptual models. Building and refining the conceptual model is essential to making meaningful interpretations of measurements. Therein lies the processes whereby measured quantities become descriptions in physically and structurally meaningful concepts.

## 6.3 Future work

The SAFE method as presented in this master's thesis can be a starting point for investigating increasingly complex structures. The method is flexible and may be applied to a wide variety of civil engineering plates and wave guides. However, the numerical scheme, in and of itself, may be refined further.

An improved method would include *generalized excitability*, as proposed by [Treyssede and Laguerre \(2013\)](#), where the excitability of evanescent modes may be computed, stringently, from the eigenvectors. Currently, only propagating modes may be computed, stringently, using *lossless excitability*. Thus, lossless excitability will only make an accurate prediction in the far-field where the contribution of evanescent modes is small. Generalized excitability overcomes this problem, and allows for a more accurate prediction of the near-field.

An important aspect of semi-analytical finite element is, that it is, in and of itself, a finite element discretisation. Hence, one can draw from the large body of previous work in constitutive modelling, element building, solution algorithms, inverse modelling and optimization that has been implemented, to enhance the method further.

In this thesis the simplest material model, isotropic linear elasticity , is used to illustrate the capabilities of SAFE. However, it is of interest to study the effects of other material models. If increasingly complex material models are introduced, in other words material models with an increasing amount of independent material parameters, some systematic treatment in updating the conceptual model is needed. Presumably, considerable insights could be drawn from optimization techniques utilized in constitutive modelling to iteratively update the model parameters.

Moreover, as in all numerical schemes, efficiency is essential. Further inquires into increased computational speed is of particular interest. In this thesis a quadratic Lagrangian element is used. One path forward could be to investigate the use of more exotic element types. Furthermore, in this thesis a single element mesh is used in solving for the wave number  $k$  for all angular frequencies  $\omega$ . However, if one has an estimate of the corresponding wave numbers to a given angular frequency, an adaptive mesh that changes for a given  $\omega$ , may be adopted. That is, the nodal points of a given mesh may be considered to be the *spatial sampling* of the displacement field, and a too fine mesh is, thus, an *over-sampling* unnecessary to accurately capture

the wave number  $k$ . Further inquiries into the marginal benefit of updating the mesh may prove to be fruitful.

Finally, the greater aim is to evaluate and refine techniques applicable to non-destructive testing (NDT). Further developments in modelling must be motivated by needs that arise from practical measurements. It is through practical measurements that non-destructive techniques become relevant, from an engineering perspective, by providing a means to evaluate structural health and make predictions about the structure's overall performance.



# Bibliography

- Achenbach, J. D., 1973. Wave Propagation in Elastic Solids, 1st Edition. Elsevier Science Publisher B.V., Amsterdam.
- Ahmad, Z. A. B., Vivar-Perez, J. M., Gabbert, U., Jan. 2013. Semi-analytical finite element method for modeling of lamb wave propagation. CEAS Aeronautical Journal 4 (1), 21–33.  
URL <http://link.springer.com/10.1007/s13272-012-0056-6>
- Auld, B. A., 1973. Acoustic fields and waves in solids. 2 volumes.
- Baggens, O., 2015. Non-Destructive evaluation of plate-like concrete structures: elatic properties and thickness. Licentiate thesis, Lund University, Faculty of Engineering.
- Baggens, O., Ryden, N., 2015. Systematic errors in Impact-Echo thickness estimation due to near field effects. NDT & E International.  
URL <http://www.sciencedirect.com/science/article/pii/S0963869514001169>
- Bartoli, I., Marzani, A., Lanza di Scalea, F., Viola, E., 2006. Modeling wave propagation in damped waveguides of arbitrary cross-section. Journal of Sound and Vibration 295 (3–5), 685–707.  
URL <http://www.sciencedirect.com/science/article/pii/S0022460X06001179>
- Boyd, A. J., Ferraro, C. C., 2005. Effect of Curing and Deterioration on Stress Wave Velocities in Concrete. Journal of Materials in Civil Engineering 17 (2), 153–158.
- Castaings, M., Lowe, M., 2008. Finite element model for waves guided along solid systems of arbitrary section coupled to infinite solid media. The Journal of the Acoustical Society of America 123 (2), 696–708.

COMSOL, 2012. User's Guide and Documentation version 4.3a. COMSOL AB.

URL [www.comsol.com](http://www.comsol.com)

Drozdz, M., Moreau, L., Castaings, M., Lowe, M., Cawley, P., 2006. Efficient numerical modelling of absorbing regions for boundaries of guided waves problems. Review of Progress in Quantitative Nondestructive Evaluation, Vols 25A and 25B 820, 126–133.

URL [http://apps.webofknowledge.com/full\\_record.do?product=WOS&search\\_mode=GeneralSearch&qid=1&SID=S18j8iQRkHWtqVL6UtU&page=1&doc=1](http://apps.webofknowledge.com/full_record.do?product=WOS&search_mode=GeneralSearch&qid=1&SID=S18j8iQRkHWtqVL6UtU&page=1&doc=1)

Fan, Z., Castaings, M., Lowe, M. J. S., Biateau, C., Fromme, P., 2013. Feature-guided waves for monitoring adhesive shear modulus in bonded stiffeners. Ndt & E International 54, 96–102.

URL <http://www.wiley.com/doi/10.1016/j.ndteint.2013.02.001>

Fan, Z., Lowe, M. J. S., 2009. Elastic waves guided by a welded joint in a plate. Proceedings of the Royal Society A: Mathematical, Physical and Engineering Sciences 465 (2107), 2053–2068.

Gohberg, I., Lancaster, P., Rodman, L., 1982. Matrix Polynomials. Academic Press, New York.

Hayashi, T., Inoue, D., 2014. Calculation of leaky Lamb waves with a semi-analytical finite element method. Ultrasonics 54 (6), 1460–1469.

URL <http://www.wiley.com/doi/10.1016/j.ultras.2014.03.001>

Hayashi, T., Song, W. J., Rose, J. L., 2003. Guided wave dispersion curves for a bar with an arbitrary cross-section, a rod and rail example. Ultrasonics 41 (3), 175–183.

URL <http://www.wiley.com/doi/10.1016/j.ultras.2003.03.001>

Ke, W., Castaings, M., Bacon, C., 2009. 3D finite element simulations of an air-coupled ultrasonic NDT system. Ndt & E International 42 (6), 524–533.

Kuttruff, H., 1998. Ultrasonics: Fundamentals and Application. Elsevier New York, New York.

Lamb, H., 1917. On waves in an elastic plate. Proceedings of the Royal Society of London (93:114).

- Lin, R., Zhu, J., Aug. 2009. On the relationship between viscous and hysteretic damping models and the importance of correct interpretation for system identification. *Journal of Sound and Vibration* 325 (1-2), 14–33.  
URL <http://www.sciencedirect.com/science/article/pii/S0022460X09002168>
- Lowe, M., 1995. Matrix techniques for modeling ultrasonic waves in multi-layered media. *Ultrasonics, Ferroelectrics, and Frequency Control*, ....  
URL [http://ieeexplore.ieee.org/xpls/abs\\_all.jsp?arnumber=393096](http://ieeexplore.ieee.org/xpls/abs_all.jsp?arnumber=393096)
- Lowe, M., Alleyne, D., Cawley, P., 1998. Defect detection in pipes using guided waves. *Ultrasonics* 36 (1-5), 147–154.
- Malhotra, V., Carino, N., 2004. *Handbook on Nondestructive Testing of Concrete*, 2nd Edition. CRC Press, Boca Raton, Florida, U.S.A.
- Neau, G., 2003. Lamb waves in anisotropic viscoelastic plates. Study of wave fronts and attenuation. Ph.D. thesis.
- Özkaya, N., Nordin, M., Goldsheyder, D., Leger, D., 2012. *Fundamentals of Biomechanics*. Springer New York, New York, NY.  
URL <http://link.springer.com/10.1007/978-1-4614-1150-5>
- Pavlakovic, B., Lowe, M., Alleyne, D., Cawley, P., 1997. Disperse: a general purpose program for creating dispersion curves. Review of progress in ....  
URL [http://link.springer.com/chapter/10.1007/978-1-4615-5947-4\\_24](http://link.springer.com/chapter/10.1007/978-1-4615-5947-4_24)
- Popovics, J., Cetrangolo, G., Jackson, N., 2006. Experimental Investigation of Impact-Echo Method for Concrete Slab Thickness Measurement.  
URL <http://www.dbpia.co.kr/Journal/ArticleDetail/3207698>
- Predoi, M. V., Castaings, M., Hosten, B., Bacon, C., 2007. Wave propagation along transversely periodic structures. *Journal of the Acoustical Society of America* 121 (4), 1935–1944.  
URL <Go to ISI>://WOS:000245687600011
- Rose, J. L., 1999. *Ultrasonic Waves in Solid Media*. Cambridge University Press, Cambridge.
- Rydén, N., 2004. Surface Wave Testing of Pavements. Ph.D. thesis, Lund.

- Ryden, N., Lowe, M. J. S., 2004. Guided wave propagation in three-layer pavement structures. *The Journal of the Acoustical Society of America* 116 (5), 2902.
- Rydén, N., Park, C. B., 2004. Surface waves in inversely dispersive media. *Near surface geophysics* 2 (4), 187–197.
- Shorter, P. J., May 2004. Wave propagation and damping in linear viscoelastic laminates. *The Journal of the Acoustical Society of America* 115 (5), 1917.  
 URL [http://apps.webofknowledge.com/full\\_record.do?product=UA&search\\_mode=GeneralSearch&qid=18&SID=Q1VSql8mfGSHvMEx8SA&page=1&doc=1](http://apps.webofknowledge.com/full_record.do?product=UA&search_mode=GeneralSearch&qid=18&SID=Q1VSql8mfGSHvMEx8SA&page=1&doc=1)
- Sondipon, A., 2000. Damping Models for Structural Vibration. Ph.d., Cambrigde University Trinity College.
- Tisseur, F., Meerberg, K., 2001. The Quadratic Eigenvalue Problem. *SIAM review* 43 (No 2), 235–286.
- Treyssede, F., Laguerre, L., 2013. Numerical and analytical calculation of modal excitability for elastic wave generation in lossy waveguides. *Journal of the Acoustical Society of America* 133 (6), 3827–3837.  
 URL <<GotoISI>://WOS:000320173600026>
- Viktorov, A. I., 1967. Rayleigh and Lamb Waves: Physical Theory and Application.
- Wilcox, P. D., Lowe, M. J. S., Cawley, P., 2001. Mode and transducer selection for long range lamb wave inspection. *Journal of Intelligent Material Systems and Structures* 12 (8), 553–565.  
 URL <<GotoISI>://WOS:000176042500005>

# Appendix: Source Code

## Sample Source Code: 1D SAFE

```
1 %  
2 %=====  
3 % 1D SAFE SAMPLE CODE FOR COMSOL MODEL  
4 %=====  
5 %=====UNIMPORTANT=====  
6 feature('DefaultCharacterSet', 'UTF8')  
7 %=====  
8  
9 import com.comsol.model.*  
10 import com.comsol.model.util.*  
11  
12 %% SAVE NAME FOR DATA FILE .mat  
13 mysaveName='modelSAVENAME';  
14  
15 %%INITIATE COMSOL MODEL  
16 model = ModelUtil.create('Model');  
17  
18 model.modelPath('C:\');  
19 model.modelNode.create('mod1');  
20  
21 model.variable.create('var1');  
22 model.variable('var1').model('mod1');  
23 % model.variable('var1').label('Variables 1: Material and  
24 % Model');  
24 model.variable.create('var2');  
25 model.variable('var2').model('mod1');  
26 % model.variable('var2').label('Variables 2: Elasticity  
27 % tensor');  
27 model.variable.create('var3');  
28 model.variable('var3').model('mod1');
```

```

29 % model.variable('var3').label('Variables 3: Stress, Strains,
30 % Power, Energy ');
31
32 %Geometry parameters
33 model.param.set('Height_1', '0.150 ', 'Height Layer 1 (
34 Concrete)');
35 model.param.set('Position_L0', '0');
36 model.param.set('Position_L1', 'Height_1+Position_L0');
37 model.param.set('Height_tot', 'Height_1','Total Height');
38
39 model.param.set('elSize1D', 'Height_tot/1000 ');
40 %Materialparameters
41 model.param.set('myrho_0', '2400 ','kg/m^3');
42
43 %Layer 1
44 model.param.set('Dfac_1', '0',' Layer 1 Damping Factor (
45 Concrete)');
46 model.param.set('myE1_0', '(myVT1^2*myrho_0*(3*myVL1^2 - 4*
47 myVT1^2))/(myVL1^2 - myVT1^2)', '[Pa] Layer 1 (Concrete)');
48 model.param.set('mynu1', '(myVL1^2 - 2*myVT1^2)/(2*myVL1^2 -
49 2*myVT1^2)', '[-] Layer 1 (Concrete)');
50 model.param.set('myE1', 'myE1_0*(1+Dfac_1)', '[Pa] Layer 1 (
51 Concrete)');
52 model.param.set('myVT1', '2635.23', '[m/s] Layer 1 (Concrete)')
53 ;
54 model.param.set('myVL1', '4303.31', '[m/s] Layer 1 (Concrete)')
55 ;
56
57 model.param.set('Freq', '1');
58 model.param.set('myomega', '2*pi*Freq');
59 model.param.set('rootSearcher', 'myomega/VTmini/2.4','Start
60 search at this wavenumber');
61 model.param.set('Fmin', '100','Lowest Frequency in frequency
62 sweep [Hz]'); %[Hz]
63 model.param.set('Fmax', '35000','Highest Frequency in
64 frequency sweep [Hz]'); %[Hz]
model.param.set('dF', '5000','Length of one step in frequency
sweep'); %[Hz]
65 %% IF USING PARAMETERIC SWEEP OVER DFAC

```

```

65 model.param.set('DFacmin', '0', 'Lowest Damping Factor in
66 damping sweep [%]');
67 model.param.set('DFacmax', '0', 'Highest Damping Factor in
68 damping sweep [%]');
69 model.param.set('dDFac', '0', 'Length of one step in damping
70 sweep');
71
72 % Boolean layered variables
73 % NB! Note that field varialbes _need_ to be variables in
74 % model variables
75 % and not global variables space.
76 model.variable('var1').set('Dfac', 'Dfac_1');
77 model.variable('var1').set('myrho', 'myrho_0');
78 model.variable('var1').set('myE', '(myE1_0*(1+i*Dfac))');
79 model.variable('var1').set('mynu', 'mynu1');
80
81 % Set energy velocity and powerflow help variables
82 % Reference Bartoli et. al .
83 % Journal of Sound and vibration 295 685-707 (2006)
84
85 % Strains (1D-strains)
86 model.variable('var3').set('e1', 'ux');
87 model.variable('var3').set('e2', '0');
88 model.variable('var3').set('e3', 'i*lambda*w');
89 model.variable('var3').set('e4', 'i*lambda*v');
90 model.variable('var3').set('e5', 'i*lambda*u+wx');
91 model.variable('var3').set('e6', 'vx');
92
93 % Stresses
94 model.variable('var3').set('Txx', 'C11*e1 + C12*e2 + C13*e3 +
95 C14*e4 + C15*e5 + C16*e6');
96 model.variable('var3').set('Tyy', 'C21*e1 + C22*e2 + C23*e3 +
97 C24*e4 + C25*e5 + C26*e6');
98 model.variable('var3').set('Tzz', 'C31*e1 + C32*e2 + C33*e3 +
99 C34*e4 + C35*e5 + C36*e6');
100 model.variable('var3').set('Tyz', 'C41*e1 + C42*e2 + C43*e3 +
101 C44*e4 + C45*e5 + C46*e6');
102 model.variable('var3').set('Txz', 'C51*e1 + C52*e2 + C53*e3 +
103 C54*e4 + C55*e5 + C56*e6');
104 model.variable('var3').set('Txy', 'C61*e1 + C62*e2 + C63*e3 +
105 C64*e4 + C65*e5 + C66*e6');
106
107 % Powerflow
108 %Reference Auld (1990) or Castaings and Lowe (2007)
109 model.variable('var3').set('Px', '0.5*real(Txx*conj(i*myomega
110 *u)+Txy*conj(i*myomega*v)+Txz*conj(i*myomega*w))');
111 model.variable('var3').set('Py', '0.5*real(Txy*conj(i*myomega
112 *u)+Tyy*conj(i*myomega*v)+Tyz*conj(i*myomega*w))';

```

```

101 model.variable('var3').set('Pz', '0.5*real(Txz*conj(i*myomega
102 *u)+Tyz*conj(i*myomega*v)+Tzz*conj(i*myomega*w))');
103 %Velocity V => du/dt = i\omega * u.
104 model.variable('var3').set('Vx', '-i*myomega*u');
105 model.variable('var3').set('Vy', '-i*myomega*v');
106 model.variable('var3').set('Vz', '-i*myomega*w');
107 %Energy expressions for an element
108 % Ec = kinetic energy, Ep = potential energy, Et = Total
109 % energy
110 model.variable('var3').set('Ec', '0.25*myrho*real(Vx*conj(Vx)
111 +Vy*conj(Vy)+Vz*conj(Vz))');
112 model.variable('var3').set('Ep', '0.25*real(Txx*conj(e1)+Tyy*
113 conj(e2)+Tzz*conj(e3)+Tyz*conj(e4)+Txz*conj(e5)+Txy*conj(
114 e6))');
115 model.variable('var3').set('Et', 'Ec+Ep');

116 %Make 1D geometry
117 model.geom.create('geom1', 1);
118
119 %layer 1
120 model.geom('geom1').feature.create('i1', 'Interval');
121 model.geom('geom1').feature('i1').set('p1', 'Position_L0');
122 model.geom('geom1').feature('i1').set('p2', 'Position_L1');

123 model.selection.create('c_dst_pc1', 'Explicit');
124 %Make a cPDE
125
126 model.physics.create('c', 'CoefficientFormPDE', 'geom1');
127 model.physics('c').field('dimensionless').component({'u' 'v'
128 'w' 'ku' 'kv' 'kw'});
129 % Sub routines for assigning an isotropic medium to the
130 % coefficient form
131 % (cPDE) environment.
132 DmatPre='myE/(1+mynu)/(1-2*mynu)*';
133 Dmat={'(1-mynu)' 'mynu' 'mynu' '0' '0' '0';
134 'mynu' '(1-mynu)' 'mynu' '0' '0' '0';
135 'mynu' 'mynu' '(1-mynu)' '0' '0' '0';
136 '0' '0' '0' '(1-2*mynu)/2' '0' '0';
137 '0' '0' '0' '0' '(1-2*mynu)/2' '0';
138 '0' '0' '0' '0' '0' '(1-2*mynu)/2'};
139 %%
140 for loopRow=1:6;
141     for loopCol=1:6;
142         string=[ 'C', num2str(loopRow), num2str(loopCol)];

```

```

142     model.variable('var2').set(string, [DmatPre,Dmat{loopRow,
143 loopCol}]);
144   end
145 end
146 % assign coefficient matrixies in coefficient PDE environment
147 model.physics('c').feature('cfeq1').set('c', {'C11'; 'C16';
148 'C15'; '0'; '0'; '0'; 'C16'; 'C66'; 'C56'; '0'; ...
149 '0'; '0'; 'C15'; 'C56'; 'C55'; '0'; '0'; '0'; '0'; ...
150 '0'; '0'; '0'; '0'; '0'; '0'; '0'; '0'; '0'; ...
151 '0'; '0'; '0'; '0'; '0'; '0'; '0'; '0'; '0'; ...
152 '0'; '0'; '0'; '0'; '0'; '0'; '0'; '0'; '0'; '-myrho*myomega^2';
153 '0'; '0'; '0'; '0'; '0'; '0'; '0'; '0'; '0'; ...
154 model.physics('c').feature('cfeq1').set('a', {'-myrho*myomega^2';
155 '0'; '0'; '0'; '0'; '0'; '-myrho*myomega^2'; '0';
156 '0'; '0'; '0'; '0'; '0'; '-myrho*myomega^2'; '0';
157 '0'; '0'; '0'; '0'; '0'; '-myrho*myomega^2'; '0';
158 '0'; '0'; '0'; '0'; '0'; '-myrho*myomega^2'; '0';
159 model.physics('c').feature('cfeq1').set('f', {'0'; '0';
160 '0'; '0'; '0'; '0'});
161 model.physics('c').feature('cfeq1').set('da', {'0'; '0';
162 '0'; '-myrho*myomega^2'; '0'; '0'; '0'; '0'; '0';
163 '-myrho*myomega^2'; '0'; '0'; '0'; '0'; '0'; '-myrho*myomega^2';
164 '-C55'; '-C45'; ...
165 '-C35'; '0'; '0'; '-C45'; '-C44'; '-C34'; '0'; '0';
166 '0'; ...
167 '-C35'; '-C34'; '-C33'; '0'; '0'; '0');
168 model.physics('c').feature('cfeq1').set('al', {'0'; '0';
169 '0'; '0'; '0'; '0'; '0'; '0'; ...
170 '0'; '0'; '0'; '0'; '0'; '0'; '0'; '0'; 'i*C15';
171 'i*C55'; '0'; '0'; '0'; '0'; '0'; '0'; '0'; '0';
172 'i*C13'; 'i*C36'; 'i*C35'; '0'; '0'; '0');
173 model.physics('c').feature('cfeq1').set('be', {'0'; '0';
174 '0'; '0'; '0'; '0'; '0'; '0'; '0'; '-i*C15';
175 '-i*C13'; '0'; '0'; '0'; '-i*C56'; '-i*C46';
176 '-i*C36'; '0'; '0'; '0'; '-i*C55'; '-i*C45';
177 '-i*C35'; '0'; '0'; '0'; '0');
178 % Create mesh
179 model.mesh.create('mesh1', 'geom1');
180 model.mesh('mesh1').feature.create('edg1', 'Edge');
181 % model.mesh('mesh1').label('Mesh');
182 % 'hauto0' 1=> extremly fine 2 => fine o.s.v.
183 model.mesh('mesh1').feature('size').set('hauto', 2);

```

```

175 %%Change to custom sized mesh
176 % model.mesh('mesh1').feature('size').set('custom', 'on');
177 % model.mesh('mesh1').feature('size').set('hmax', 'elSize1D')
178 ;
179 model.mesh('mesh1').run;
180
181 % Get mesh shape and mesh statistics
182 mphmesh(model,'mesh1');
183 figure(1);
184 meshstats = mphmeshstats(model)
185 mphmesh(model,'mesh1');
186
187 model.study.create('std1');
188 model.study('std1').feature.create('eigv', 'Eigenvalue');
189 model.study('std1').feature.create('param', 'Parametric');
190
191 model.study('std1').feature('param').set('pname', {'Freq'});
192 model.study('std1').feature('param').set('plistarr', {'range(
    Fmin,dF,Fmax)'});
193 model.study('std1').feature('eigv').set('shift', '
    rootSearcher');
194 model.study('std1').feature('eigv').set('neigs', '100');
195 %%
196 model.study('std1').run;

```